HAL
open science

Density-based phase envelope construction including capillary pressure

Dan Vladimir Nichita

To cite this version:

Dan Vladimir Nichita. Density-based phase envelope construction including capillary pressure. Fluid Phase Equilibria, 2019, 498, pp.33-44. 10.1016/j.fluid.2019.06.018 . hal-02379737

HAL Id: hal-02379737

https://hal.science/hal-02379737v1

Submitted on 17 Dec 2020

HAL is a multi-disciplinary open access archive for the deposit and dissemination of scientific research documents, whether they are published or not. The documents may come from teaching and research institutions in France or abroad, or from public or private research centers.

L'archive ouverte pluridisciplinaire **HAL**, est destinée au dépôt et à la diffusion de documents scientifiques de niveau recherche, publiés ou non, émanant des établissements d'enseignement et de recherche français ou étrangers, des laboratoires publics ou privés.

Density-based phase envelope construction including capillary pressure

Dan Vladimir Nichita [1,*]

[1] *CNRS UMR 5150, Laboratoire des Fluides Complexes et leurs Réservoirs, Université de Pau et des Pays de l'Adour, B.P. 1155, 64013 Pau Cedex, France*

Abstract

A recently proposed density-based phase envelope construction method (Nichita, Fluid Phase Equilib. 478, 100-113, 2018) is adapted to account for capillary effects. The set of saturation point equations is selected such as both the zero tangent plane distance (TPD) function (in terms of component molar densities and temperature) and the Young-Laplace equation are honored. The set of variables and potential specifications includes mixture molar density, temperature and the modified equilibrium constants (defined as the ratios of reference to incipient phase component molar density). The number of equations and the variables are the same as in the bulk fluid case. The density-based method including capillary pressure is not dependent on the thermodynamic model; any pressure-explicit equation of state and volume-explicit interfacial tension model can be used. The equation of state (EoS) must not be solved for volume and the elements of the Jacobian matrix have simpler expressions than those in conventional (pressure-based) methods. A code for phase envelope construction of bulk fluids can be easily modified by adding the capillary terms to the residual functions and Jacobian matrix. The additional partial derivatives of capillary terms have very simple expressions due to the explicit in volume form of the interfacial tension model. Unlike in conventional formulations, negative pressures in the reference phase can be handled. The proposed method is tested for several hydrocarbon mixtures, ranging from natural gases to heavy oils. As compared to a bulk fluid, under capillary pressure influence the bubble point pressures are suppressed and the dew point locus is expanded, with a shift of cricondentherm points towards higher temperatures. For the mixtures investigated, the computational results are practically identical to those reported in the literature. The computational procedure is robust, there are no problems neither in crossing the critical region (where interfacial tensions are very low) nor at important negative pressures and for very large capillary pressures (of the order of hundreds bar in some test examples).

Keywords: phase envelope, capillary pressure, interfacial tension, tangent plane distance, volume-based method, molar density, Newton method

---

* Address correspondence to Dan Vladimir Nichita, E-mail: dnichita@univ-pau.fr

1. Introduction

Saturation point calculations represent one of the basic phase equilibrium calculation problems. Phase envelopes are the fingerprint of a mixture of given composition in the planes defined by state variables or functions. Even though several stand-alone saturation point calculation procedures have been proposed [1-3], the safest procedure is to trace the entire phase envelope using continuation methods [4,5], by calculating the entire family of solutions, starting from an "easy" point where a non-problematic convergence can be obtained (such as a low-pressure dew or bubble point). The most widely used approach is the one presented by Michelsen (1980) [4]. Several variations of this kind of procedure have been proposed [6-10], using conventional (PT, or pressure-based) methods (with the Gibbs free energy as the central thermodynamic potential), in which the volume is a dependent variable and is calculated from the equation of state at given pressure, temperature and composition.

In volume-based thermodynamics (in which the Helmholtz free energy is the central thermodynamic potential), volume, temperature and mole numbers (which are the natural variables in a pressure-explicit equation of state) [11], or molar densities and temperature [12,13] are the primary variables. Whatever the type of phase equilibrium calculations (phase stability phase splitting, saturation points), the main advantages of volume-based methods are that the EoS is not solved for volume, simpler partial derivatives are required and calculations can be also performed at negative pressures. A disadvantage of volume-based methods is that successive substitutions (SSI) cannot be used (even if the SSI method can be formulated, it is not robust as in the conventional PT formulation [14-16]), thus robust modified Newton methods [15-19] or very good initial guesses for a full Newton method (as in automated phase envelope construction) are required. Volume-based methods are slightly slower than the conventional ones in terms of number of iterations required for convergence [16,19], but the computational cost of an iteration is lower. Volume-based phase envelope construction methods were presented by Kunz et al. [20], Quinones-Cisneros and Deiters [21], Deiters [22], Bell and Deiters [23] and Nichita [24]. A density marching method [10] (although not properly speaking a volume-based method) used density as an independent variable and constructed phase envelopes by monotonically varying the density of the feed.

Saturation point calculations are closely related to phase stability testing [25] in both conventional and volume-based approaches. At a saturation point, the tangent plane distance function equals zero and is at its non-trivial global minimum for the incipient phase composition [26]. In all saturation point calculation methods, the set of equations is selected in such a manner that both

equilibrium (of the reference phase with an incipient phase) and zero TPD function conditions are satisfied.

It is well known that capillarity affects fluid phase behavior in porous media and its influence increases with curvature; capillary effects are very important in nanopores. As compared to a bulk fluid, under capillary pressure influence the bubble point pressures are suppressed and the dew point locus is inflated (showing an increase of retrograde dew point pressures and a decrease of lower dew point pressures), with a shift of cricondentherm points towards higher temperatures [27-30].

In phase equilibrium calculations with capillary pressure influence, the equilibrium equations (equality of chemical potentials) are solved together with the capillary pressure (Young-Laplace) equation (Shapiro and Stenby [27], Brusilovski [31]). Phase equilibrium calculations including capillary pressure received considerable attention in the last few years, mainly related to the increased interest of the petroleum and gas industry and research in the development of shale oil and gas reservoirs. Many papers present mixture phase envelopes and the influence of capillarity on phase boundaries using conventional (pressure-based) methods. In most of them, saturation points are indirectly calculated from flash calculations or stability testing; such a procedure is tedious (with possible problems near critical points) and calculations at many points are required to achieve a good precision. However, only in few papers a direct calculation of saturation points is reported (Brusilovski [31], Nojabaei et al. [32], Pang et al. [33], Li et al. [34]) and even fewer are presenting an automated construction of phase envelopes including capillary pressure (Sandoval et al. [28] and Zuo et al. [35]).

Recently, phase envelopes with capillary pressure influence were indirectly constructed using volume-based methods by VT (at constant volume, temperature and moles) flash calculations by Li et al. [30] and by Lu et al. [36]; in the latter work phase boundaries are drawn in the molar density-temperature (d-T) plane. Sandoval et al. [37] presented an automated volume-based method for phase envelope construction.

In this paper, a density-based phase envelope construction including capillary pressure is proposed. It is shown how a recent calculation method for bulk fluids (Nichita [24]) can be readily adapted to include the capillary effects by simple modifications of the residual functions and Jacobian matrix; the partial derivatives including capillary terms have very simple expressions, since the interfacial tension model is explicit in molar densities (this represents an additional advantage of volume- or density-based methods if capillarity is taken into account). Geometrical confinement and adsorption are not addressed here.

The paper is organized as follows. First, the tangent plane distance function in terms of molar densities and temperature and the equations of saturation point calculations are presented for both bulk fluids (section 2) and with capillary effects (section 3), then the phase envelope construction including capillary pressure is presented, with emphasis to the treatment of additional capillary terms (section 4). Several examples of various phase envelope construction (ranging from natural gases to heavy oils) without/with capillary pressure at different capillary radii are presented and discussed (section 5) before concluding.

2. Saturation points of a bulk fluid

Saturation point calculations are closely related to phase stability testing; one way or another, the saturation point equations are selected to ensure that a TPD function equals zero. In volume-based methods for stability testing, the TPD function can be expressed at given temperature either in terms of mole numbers and volume [14,16,18,25] or of molar densities [12,13,14,38,39]. A volume-based stability criterion was proposed for the first time by Nagarajan et al. [12], with component molar densities and temperature as primary variables. The TPD function is

$$D(\mathbf{d},T)=\sum_{i=1}^{nc} d_i\left[\ln f_i(\mathbf{d},T)-\ln f_{iz}(\mathbf{d_z},T)\right]-\frac{P(\mathbf{d},T)-P_z(\mathbf{d_z},T)}{RT} \qquad (1)$$

where $\mathbf{d}$ is the vector of component molar densities in the trial phase, $\mathbf{d}=(d_1,...,d_{nc})^T$, with $d_i=n_i/V=x_i d$ and the index z corresponds to the feed (reference phase) of molar densities $d_{iz}=n_{iz}/V_z=z_i d_z; i=1,nc$, with $n_{iz}=n_T z_i$.

In phase stability testing, the feed molar density, d_z, is always fixed; it is directly related to the specifications ($d_z=n_T/V_z=1/v_z$) in VT (at constant volume, temperature and moles) stability testing or it is directly calculated from the EoS at the specifications in conventional PT (at constant pressure and temperature) stability testing. Since the feed composition is fixed in all calculations, from here the vector $\mathbf{z}$ is dropped from all argument lists (this also means that the vector $\mathbf{d_z}$ is replaced by d_z in these lists).

A mixture is stable at given temperature T if $D\geq 0$ for all feasible $\mathbf{d}$ (the global minimum is zero); if for some $\mathbf{d}$ the TPD function $D<0$, the mixture is unstable and it splits in two (or more) phases.

Several volume-based calculation methods have been proposed for phase stability testing using the TPD function in Eq. (1), for both VT stability testing [14,15,18,39] and PT stability

[12,19,38] testing, using either global optimization methods [18,38,39] or local minimization (modified Newton) methods starting from several initial guesses [14,15,18,19].

At the saturation points, the following equations must be satisfied [24]

$$\Phi_i(\mathbf{d}, d_z, T) = \ln f_i(\mathbf{d}, T) - \ln f_{iz}(d_z, T) = 0; i = 1, nc \tag{2}$$

and

$$\Phi_{nc+1}(\mathbf{d}, d_z, T) = \frac{P(\mathbf{d}, T) - P_z(d_z, T)}{RT} = 0 \tag{3}$$

Here **d** is the vector of molar densities of the incipient phase and d_z can be either a variable or a specification (the latter for saturation temperature calculations at given molar density or volume). The denominator in Eq. (3) is kept for scaling purposes.

The RHS of Eq. (2) is the gradient of the TPD function in Eq. (1) [14-16], thus any values of **d**, d_z and T satisfying Eq. (2) define a stationary point. Moreover, from equations (2) and (3), the TPD function is zero. A non-trivial solution of the nonlinear system of nc+1 equations (2) and (3) corresponds to a point on the phase boundary, with a non-trivial (global) minimum of the TPD function (see Ref. [24], where a detailed discussion can be found). Equations (2) and (3) represent the starting point of the recently proposed method for density-based phase envelope construction for a bulk fluid by Nichita [24].

3. Saturation points with capillary pressure

In any type of phase equilibrium calculation in the presence of capillary effects (stability, flash or saturation point calculations), the thermodynamic equilibrium equations (the equality of chemical potentials) are solved together with the capillary pressure equation.

The capillary pressure P_C is given by the Young-Laplace equation

$$P_C = P_V - P_L = \frac{2\sigma\cos\theta}{r} \tag{4}$$

where σ is the interfacial tension, r is the capillary radius and θ is the contact angle of the meniscus with the pore wall.

The interfacial tension relation of Macleod [40] and Sugden [41] was extended to mixtures by Weinaug and Katz [42]

$$\sigma^{1/E} = \sum_{i=1}^{nc} \Pi_i \left(x_i d_L - y_i d_V \right) = \sum_{i=1}^{nc} \Pi_i \left(d_{iL} - d_{iV} \right) \tag{5}$$

where Π_i is the parachor of component *i*, *E* is a scaling factor and *d* is the phase molar density. The scaling factor is $E = 4$ [42] (various other values were proposed for *E*, ranging from 3.66 ton 3.91 [43]).

The limit of validity of the parachor model for interfacial tensions given by several authors [32,44] is *r*=5 nm. Moreover, at small capillary radii, the role of confinement and adsorption (not addressed here) is predominant. In this paper, we assume that calculations performed at $r \geq 5\,\text{nm}$ can be considered physically correct; however, in some numerical experiments, a smaller capillary radius (*r*=2 nm) will be also considered to test the robustness of the proposed calculation method at very high curvature (or capillary pressure).

For phase stability testing and saturation point calculations, the interfacial tension is expressed as [45]

$$\sigma(\mathbf{d}, d_z) = \left(\sum_{i=1}^{nc} \gamma \Pi_i \left(z_i d_z - d_i \right) \right)^E \tag{6}$$

thus the capillary pressure is a function of only **d** and d_z, $P_C = P_C(\mathbf{d}, d_z)$. Whichever the reference phase, vapor or liquid, Eq. (6) is equivalent to Eq. (5) for $\gamma = \pm 1$.

The values of γ are $\gamma = -1$ on the dew point side of the phase boundary (the reference phase is vapor and the incipient phase is liquid) and $\gamma = +1$ on the bubble point side of the phase boundary (the reference phase is liquid and the trial phase is vapor); $\gamma = 0$ corresponds to the bulk fluid.

The TPD function in terms of component molar densities including capillary pressure is (Kou and Sun [46])

$$D(\mathbf{d}, d_z, T) = \sum_{i=1}^{nc} d_i \left[\ln f_i(\mathbf{d}, T) - \ln f_{iz}(d_z, T) \right] - \frac{P(\mathbf{d}, T) - P_z(d_z, T)}{RT} + \gamma \frac{P_C(\mathbf{d}, d_z)}{RT} \tag{7}$$

The set of equations for saturation point calculations is

$$\Phi_i(\mathbf{d}, d_z, T) = \ln f_i(\mathbf{d}, T) - \ln f_i(d_z, T) = 0; i = 1, nc \tag{8a}$$

and

$$\Phi_{nc+1}(\mathbf{d}, d_z, T) = \frac{P(\mathbf{d}, T) - P_z(d_z, T) - \gamma P_C(\mathbf{d}, d_z)}{RT} = 0, \tag{8b}$$

The solution of the non-linear system of equations, equations (8a) and (8b): i) ensures a zero value of the TPD function; ii) honor the Young-Laplace equation, but iii) it does not correspond to a minimum of the TPD function (Eq. 7), in the sense that Eq. (8a) is not the stationarity condition of the TPD function in the space defined by **d** and *T*, and iv) is consistent with indirect solutions from conventional phase stability (which is not a minimum of the TPD function) and flash calculations (which is not a not minimum of the Gibbs free energy).

In fact, for any type of phase equilibrium calculations including capillary pressure, the residual functions are not the gradient of the objective function including capillary effects (the dependence of the capillary pressure on mole numbers or molar densities is not accounted for in the differentiation) and are formally identical to the gradient (thermodynamic equilibrium equations) in the bulk fluid case. Thus, a phase equilibrium problem including capillary pressure is usually not solved as a minimization problem, but as an equation solving problem, with a non-symmetric Jacobian matrix [29,31,37].

If a direct minimization of the TPD function in Eq. (7) is performed, as in Kou and Sun (using an evolutionary method) [46] and Nichita (using a modified Newton method) [45], the dependence of capillary pressure on molar densities is considered in the gradient, which contains the derivative $\partial P_C / \partial d_i$; the main advantage of the minimization approach is that symmetry can be used both in constructing the Hessian matrix and in controlling the decrease of the objective function. There are some (generally slight) differences between the equation-solving (conventional and volume-based) results and those of the minimization approach for phase stability, as discussed in Ref. [45]. As mentioned, in this work, the saturation point equations correspond to the equation solving approach and the results are identical to those obtained by any conventional or similar volume-based methods, since the same system of equations (containing the thermodynamic equilibrium equations and the capillary pressure equation) is solved for different independent variables at different specifications (see also Ref. [37]).

4. Phase envelope construction with capillary pressure

4.1. Thermodynamic functions and variables

When working with molar densities, it is more convenient to use a density function instead of fugacity coefficients. The density function is defined as

$$\Psi_i(\mathbf{d},T)=\frac{f_i(\mathbf{d},T)}{d_i} \tag{9}$$

and was introduced [15] to isolate molar densities in the stationarity conditions of the TPD function (Eq. 2).

The modified equilibrium coefficients were defined as the ratio of the feed to incipient phase molar densities [24]

$$\overline{K}_i=\frac{d_{iz}}{d_i} \tag{10}$$

From equations (8a), (9) and (10), $\overline{K}_i$ is

$$\overline{K}_i=\frac{\Psi_i(\mathbf{d},T)}{\Psi_{iz}(d_z,T)} \tag{11}$$

From the above equation, it can be seen that in the density-based method, the modified equilibrium constants replace equilibrium constants in $K_i=\varphi_i/\varphi_{iz}$ and the density function replace the fugacity coefficients, as compared to the conventional PT method. In density-based saturation point calculations, the natural logarithms of the modified equilibrium constants (which are unbounded) can be used as independent variables (or one of them as a specification) instead of the component molar densities (which are bounded).

From Eq. (10) and $d_{iz}=z_i d_z$, at fixed feed composition the component molar densities depend only on the modified equilibrium constants and on the molar density of the feed.

$$\ln d_i=-\ln\overline{K}_i+\ln d_z+\ln z_i \tag{12}$$

Eq. (12) is a key equation, relating the thermodynamic functions of molar densities to the independent variables. The partial derivatives of molar densities with respect to these variables are

$$\frac{\partial d_i}{\partial \ln\overline{K}_j}=\delta_{ij}d_i;i,j=1,nc \tag{13}$$

and

$$\frac{\partial d_i}{\partial d_z} = \frac{d_i}{d_z}; i = 1, nc \tag{14}$$

Taking into account Eq. (10), the density functions

$$\Psi_i(\mathbf{d}, T) = \Psi_i\left[\mathbf{d}(\mathbf{ln}\overline{\mathbf{K}}, d_z), T\right] = \Psi_i(\mathbf{ln}\overline{\mathbf{K}}, d_z, T) \tag{15a}$$

where $\mathbf{ln}\overline{\mathbf{K}} = (\ln \overline{K}_1, ..., \ln \overline{K}_{nc})^T$ and the pressure

$$P(\mathbf{d}, T) = P\left[\mathbf{d}(\mathbf{ln}\overline{\mathbf{K}}, d_z), T\right] = P(\mathbf{ln}\overline{\mathbf{K}}, d_z, T) \tag{15b}$$

depend on $\ln \overline{K}_i$, feed molar density and temperature.

For a fixed feed composition **z**, the thermodynamic functions depend only on feed molar density and temperature, that is,

$$\Psi_{iz}(\mathbf{d_z}, T) = \Psi_{iz}(\mathbf{n_z}, d_z, T) = \Psi_{iz}(d_z, T) \tag{16a}$$

and

$$P_z(\mathbf{d_z}, T) = P_z(\mathbf{n_z}, d_z, T) = P_z(d_z, T) \tag{16b}$$

The capillary pressure depends (at fixed capillary radius and contact angle) only on **d** and d_z, via the interfacial tension, and can be written as

$$P_C(\mathbf{d}, d_z) = P_C\left[\mathbf{d}(\mathbf{ln}\overline{\mathbf{K}}, d_z), d_z\right] = P_C(\mathbf{ln}\overline{\mathbf{K}}, d_z) \tag{17}$$

These dependences are used later in the chain rule to obtain the required partial derivatives.

The chemical potential and the pressure are first-order homogenous functions of mole numbers and volume (at constant temperature). Applying Euler's theorem on homogeneous functions

$$\sum_{i=1}^{nc} n_i \frac{\partial \mu_i}{\partial n_j} + V \frac{\partial \mu_j}{\partial V} = 0; j = 1, nc \tag{18a}$$

and

$$\sum_{i=1}^{nc} n_i \frac{\partial P}{\partial n_i} + V \frac{\partial P}{\partial V} = 0 \tag{18b}$$

In terms of molar density, taking into account that $d = n/V = 1/v$ and the symmetry of second-order partial derivatives of the Helmholtz fee energy ($\partial \ln f_i / \partial V = (\partial P / \partial n_i)/RT$, expressed as $\partial \ln f_i / \partial d = (\partial P / \partial d_i)/dRT$), the above equations read

$$\sum_{i=1}^{nc} d_i \frac{\partial \ln f_i}{\partial d_j} - \frac{1}{RT}\frac{\partial P}{\partial d_j} = 0;\ j = 1, nc \tag{19a}$$

and

$$\sum_{i=1}^{nc} d_i \frac{\partial P}{\partial d_i} - d\frac{\partial P}{\partial d} = 0 \tag{19b}$$

In the differentiation process to obtain the partial derivatives required to build the Jacobian matrix, the chain rule (in Eqs. 15 to 17), as well as the homogeneity and symmetry properties (in Eqs. 19) are taken into account.

4.2. Resolution of the nonlinear system of equations

The vector containing the *nc*+1 independent variables and one specification is $\boldsymbol{\xi} = \left(\ln \overline{K}_1, \ldots, \ln \overline{K}_{nc}, \ln d_z, \ln T\right)^T$. The nonlinear system of equations is

$$\Phi_i\left(\mathbf{ln}\overline{\mathbf{K}}, d_z, T\right) = \ln \Psi_i\left(\mathbf{ln}\overline{\mathbf{K}}, d_z, T\right) - \ln \Psi_{iz}\left(d_z, T\right) - \ln \overline{K}_i = 0;\ i = 1, n \tag{20a}$$

$$\Phi_{nc+1}\left(\mathbf{ln}\overline{\mathbf{K}}, d_z, T\right) = \frac{P\left(\mathbf{ln}\overline{\mathbf{K}}, d_z, T\right) - P_z\left(d_z, T\right) - \gamma P_C\left(\mathbf{d}, d_z\right)}{RT} = 0 \tag{20b}$$

$$\Phi_{nc+2} = \xi_k - S = 0 \tag{20c}$$

where ξ_k is the specification and S the fixed value of the specification (the index k indicates the position of the specification in the vector of variables $\boldsymbol{\xi}$; for example if d_z is fixed, k=nc+1).

Note that in saturation point calculations with capillary pressure, the number of equations and the unknowns are the same as in the bulk case.

As compared with the corresponding equation for the bulk fluid, Eq. (20b) reads

$$\Phi_{nc+1}^{(cap)} = \Phi_{nc+1}^{(bulk)} - \gamma \frac{P_C}{RT} \tag{21}$$

that is, the only difference is that the capillary pressure is added to the *nc*+1 element in the vector of residuals.

The linear system of equations in the Newton method is, in matrix form

$$\mathbf{J}\Delta\boldsymbol{\xi} = -\Phi \tag{22}$$

and the elements of the Jacobian matrix are

$$J_{ij} = \frac{\partial \Phi_i}{\partial \ln \overline{K}_j} = -\delta_{ij} - d_j \left(\frac{\partial \ln \Psi_i}{\partial d_j} \right)_{T, d_{s \neq j}} ; i, j = 1, nc \tag{23a}$$

$$J_{i,nc+1} = \frac{\partial \Phi_i}{\partial \ln d_z} = \frac{1}{RT} \left[\left(\frac{\partial P}{\partial d_i} \right)_{T, d_{s \neq i}} - \left(\frac{\partial P_z}{\partial d_{zi}} \right)_{T, d_{z,s \neq i}} \right]; i = 1, nc \tag{23b}$$

$$J_{i,nc+2} = \frac{\partial \Phi_i}{\partial \ln T} = T \left[\left(\frac{\partial \ln \Psi_i}{\partial T} \right)_{\mathbf{d}} - \left(\frac{\partial \ln \Psi_{iz}}{\partial T} \right)_{\mathbf{d_z}} \right]; i = 1, nc \tag{23c}$$

$$J_{nc+1,j} = \frac{\partial \Phi_{nc+1}}{\partial \ln \overline{K}_j} = -\frac{d_j}{RT} \left(\frac{\partial P}{\partial d_j} \right)_{T, d_{s \neq j}} - \frac{\gamma}{RT} \left(\frac{\partial P_C}{\partial \ln \overline{K}_j} \right)_{T, d_z} ; j = 1, nc \tag{23d}$$

$$J_{nc+1,nc+1} = \frac{\partial \Phi_{nc+1}}{\partial \ln d_z} = \frac{1}{RT} \left[d \left(\frac{\partial P}{\partial d} \right)_{T, \mathbf{n}} - d_z \left(\frac{\partial P_z}{\partial d_z} \right)_{T, \mathbf{n_z}} \right] - \frac{\gamma}{RT} \left(\frac{\partial P_C}{\partial \ln d_z} \right)_{T, \mathbf{d}} \tag{23e}$$

$$J_{nc+1,nc+2} = \frac{\partial \Phi_{nc+1}}{\partial \ln T} = \frac{1}{R} \left[\left(\frac{\partial P}{\partial T} \right)_{\mathbf{d}} - \left(\frac{\partial P_z}{\partial T} \right)_{\mathbf{d_z}} - \frac{P - P_z}{T} \right] - \frac{\gamma}{R} \left(\frac{\partial (P_C / T)}{\partial \ln T} \right)_{d_z, \mathbf{d}} \tag{23f}$$

and

$$J_{nc+2,j} = \frac{\partial \Phi_{nc+2}}{\partial \xi_j} = \delta_{jk} ; j = 1, nc+2 \tag{23g}$$

In the first term is the RHS of Eq. (23e), a misprint in Ref. [24] is corrected; if $\gamma = 0$, the above equations correspond to the bulk fluid case [24].

The Jacobian matrices without/with capillary pressure influence are related by $\mathbf{J}^{(cap)} = \mathbf{J}^{(bulk)} + \mathbf{C}$, or

$$J_{ij}^{(cap)} = J_{ij}^{(bulk)} + C_{ij} ; i, j = 1, nc \tag{24}$$

The interfacial tension is $\sigma = \sigma(\mathbf{d}, d_z)$ and the partial derivatives of the capillary pressure with respect to molar densities and temperature are

$$\left(\frac{\partial P_C}{\partial d_i} \right)_{d_{j \neq i}, d_z, T} = \gamma \frac{2 \cos\theta}{r} E \sigma^{\frac{E-1}{E}} \Pi_i ; i = 1, nc \tag{25}$$

and

$$\left(\frac{\partial P_C}{\partial T}\right)_{\mathbf{d},d_z} = 0 \tag{26}$$

The matrix **C** contains capillary terms and has non-zero elements only on the row *nc*+1 ($C_{ij} = 0; i = 1, nc; i = nc + 2;\ j = 1, nc$). The elements of this row are

$$C_{nc+1,j} = -\frac{\gamma}{RT}\left(\frac{\partial P_C}{\partial \ln \overline{K}_j}\right)_{T,d_z} = \frac{2\cos\theta}{r}\frac{1}{RT}E\sigma^{\frac{E-1}{E}}\Pi_j d_j;\ j = 1, nc \tag{27a}$$

$$C_{nc+1,nc+1} = -\frac{\gamma}{RT}\left(\frac{\partial P_C}{\partial \ln d_z}\right)_{T,d_z} = -\frac{2\cos\theta}{r}\frac{\gamma}{RT}E\sigma = -\frac{\gamma E}{RT}P_C \tag{27b}$$

and

$$C_{nc+1,nc+2} = -\frac{\gamma}{R}\left(\frac{\partial(P_C/T)}{\partial \ln T}\right)_{d_z,\mathbf{d}} = -\frac{\gamma}{RT}P_C \tag{27c}$$

where equations (25) and (26) were used in the differentiation.

Note the extremely simple expressions of the above derivatives (which are calculated at practically no extra computational cost as compared to the bulk case), due to the explicit form in molar density of the interfacial tension model; this property makes volume-based methods particularly suited for phase equilibrium calculations including capillary pressure. A density-based Newton iteration is clearly faster than a conventional (PT) one, because the EoS is not solved for volume, there is no root selection procedure and the partial derivatives are substantially simpler.

4.3. Phase envelope construction

The density-based phase envelope calculation procedure is the same as the one for the bulk fluid (described in detail in Nichita [24]), which follows Michelsen's [4] framework (also extended by Sandoval et al. [28,37] to include capillary effects) to automatically calculate the entire family of solutions in a single run.

High quality initial guesses are available at each point on the phase envelope. The linear system of equations

$$\mathbf{J}\frac{\partial \xi}{\partial S} = -\frac{\partial \Phi}{\partial S} \tag{28}$$

is solved, where $\partial\Phi / \partial S = (0,0,...,0,-1)^T$, and its solutions are used to perform linear (at the first point) and cubic (at subsequent points) extrapolations. The most sensitive variable is selected as the specification at the next step.

Calculations start at an "easy" point where a non-problematic convergence can be obtained, such as a dew point (DP) temperature calculation at a low pressure (10-20 bar) or at a small feed molar density (e.g., d_z=0.1 Kmol/m^3). The EoS is solved for volume only for initialization at the first point and initial guesses of equilibrium constants are obtained from Wilson's [47] relation. Note that for the first point, density-based iterations are also used in this work, unlike in Sandoval et al. [37] where traditional PT-based iterations are used. The remaining part of the saturation curve can be drawn in the opposite direction (i.e., by increasing the logarithm of the most volatile component or by decreasing the feed molar density for the low pressure part of the lower dew point curve). A bubble point (BP) temperature calculation at low pressure can also be used for the first point; for usual (closed) phase envelopes the results are the same for both DP and BP initial points, but unstable branches of the phase envelope can be found starting from a BP [4,20,24].

No computational problems were observed in crossing critical points where the algorithm keeps its robustness shown for bulk fluids [24]; interfacial tensions are very small in the neighborhood of a critical point (where they vanish) and small on a relatively large part of the phase boundary, where the algorithm behaves almost like in the bulk fluid case.

Far from the critical point, where capillary pressures may become important (as in most examples in the next section), there are no computational problems neither at high capillary pressures, nor at important negative pressures in the reference phase on the bubble point side of the phase envelope.

The equations of temperature (in d-T and T-P planes) and pressure (in the T-P plane) extrema are the same as for the bulk fluid [24], with the capillary terms included in equations (23d) and (23e).

It can be noted that the partial derivatives at constant temperature required to assemble the Jacobian matrix are with respect to molar densities. For any EoS, these derivatives are usually given with respect to mole numbers and volume. It was shown in Nichita [15,24], that due to homogeneity properties, the existing routines (in mole numbers and volume) need not to be modified and can be called to calculate the required functions and partial derivatives. All the required relations between functions and their partial derivatives expressed in terms of molar densities and those expressed in mole numbers and volume are given in Ref. [24].

5. Results and discussion

The proposed method is tested for several representative hydrocarbon mixtures, ranging from natural gases to heavy oils. A general form of two-parameter cubic EoS (containing the forms of SRK EoS [48] and PR EoS [49,50]) is used in all calculations (see Ref. [24] for the EoS, thermodynamic functions and required partial derivatives). In the interfacial tension model, the scaling factor is $E = 4$ and the contact angle is taken $\theta = 0$ (complete liquid-wetting) in all calculations.

Data for all mixtures (composition, component properties and non-zero binary interaction parameters) are given in a supplementary material (**Tables S1** to **S5**). Saturation point calculations are performed between a very small d_z and a molar density very close to $d_{\max} = 1/v_{\min}$, corresponding to the covolume of the reference phase, $v_{\min} = b_z = \sum_{i=1}^{nc} b_i z_i$. Mixture phase boundaries are shown in both T-P and d-T planes for the bulk fluid and for different capillary radii. The properties of the critical points (temperature, pressure and molar density) for all mixtures are listed in **Table 1**.

5.1. M7 natural gas

A natural gas from Michelsen [25], containing 7 components (normal alkanes from C_1 to nC_6 and nitrogen), denoted here M7, with component properties and non-zero binary interaction parameters (BIPs) from Ref. [28] given in **Table S1**. The SRK EoS is used (as in Refs. [28] and [37]) and calculations are performed at three capillary radii, r=10 nm, r=5 nm and r=2 nm; the latter capillary radius is included to evaluate the capabilities of the algorithm to handle such conditions at very high curvatures.

The phase boundaries of the bulk fluid and with capillary pressure influence are plotted in the d-T plane in **Fig. 1a**, with a detail at high temperatures around the cricondentherm point in **Fig. 1b** and in the T-P plane (including the negative pressures domain) in **Fig. 2a**, with a detail in **Fig. 2b**, showing also the pressure of the incipient (here liquid) phase, noted P_w; the pressure of the reference phase is noted P_z. The bubble point pressures are suppressed, the upper (retrograde) dew point pressures are increased, while the lower dew point pressures are decreased by capillary effects; the cricondentherm points are displaced towards higher temperatures. For r=10 nm, the results are identical with those reported in Ref. [28] for several selected points on the phase envelope.

The largest capillary pressures in this example, as well as the largest negative pressures exceed 100 bar for r=2 nm, both at low temperatures and on the dew point side of the phase boundary. The cricondentherm points are shifted with 5 K for r=5 nm and with 12 K for r=2 nm.

The branch of negative pressures P_w (incipient liquid phase) at high temperatures can be handled by conventional PT methods since P_z (vapor) is positive (as for instance in Sandoval et al. [28]). However, the portion of the saturation curve at low temperature for negative pressure P_z (liquid reference phase) cannot be handled by conventional PT methods, but there is not any problem in volume-based methods, even at very high capillary pressure differences and very large negative values of the pressure P_z.

The incipient phase molar density is plotted vs. feed molar density in **Fig. 3**. Differences in density seem to be less important than those in pressure; however, relative deviations up to 50 % can be observed at large densities. The less usual representation of the pressure in function of molar density (with a unique pressure at fixed molar density) is given in **Fig. 4**, showing both reference and incipient phase pressures.

5.2. SJ15 oil and gas condensate

Two mixtures (denoted here SJ15 Oil and SJ15 gas condensate) were used as test mixtures by Sherafati and Jessen [29] to study phase stability testing with capillary pressure. The mixtures are described with 15 components (with 5 heavy pseudo-components), of compositions, component properties and BIPs [29] listed in **Table S2**.

Calculations for the SJ15 Oil are performed using the SRK EoS, for the capillary radii of r=10 nm and r=5 nm (as in Ref. [29]). The phase envelopes of SJ15 oil are plotted in **Fig. 5a** in the d-T plane (with a detail in **Fig. 5b**) and in **Fig. 6** in the T-P plane. Details of the phase envelopes in the T-P plane are presented in **Fig. 7a** (on the dew point side) and in **Fig7b** (on the bubble point side). The results are identical to those in Ref. [29] and match those in Ref. [45], obtained using the conventional approach by indirect calculation of saturation points from stability testing.

The cricondentherm points shift is from 9 K (r=10 nm) to 17 K (r=2 nm); capillary pressures and negative pressures (P_z) on the bubble point side are very noticeable, greater than 250 bar at r=2 nm.

The phase envelopes of the SJ15 gas condensate, calculated with the SRK EoS, are presented in **Fig. 8a** in the d-T plane (with a detail around the cricondentherm point in **Fig. 8b**) and **Fig. 9a** (with a detail in **Fig. 9b**) in the T-P plane, for there capillary radii (r=10 nm, r=5 nm [29,37] and r=2 nm [37]). The stability of the algorithm is not affected by the presence of only traces of the three heaviest pseudo-components. The cricondentherm points exhibit an important shift, with 12 K at r=10 nm, with

24 K at r=5 nm and with 52 K at r=2 nm. The results are the same as those in Refs. [29] (for $r \geq 5\,\text{nm}$) and [37], but here P_w is also shown, with negative pressures exceeding 250 bar. The maximum negative value of P_z is also important.

5.3. Eagle Ford oil

The composition of the Eagle Ford oil mixture is described with 14 components (including 4 heavy pseudo-components). Composition and component properties (see **Table S3**) and non-zero BIPs (see **Table S4**) are taken from Orangi et al. [51]. The SRK EoS is used (as in Ref. [37]).

Calculations are performed for the capillary radii of r=10 nm, r=5 nm and again, r=2 nm to test the robustness at very high curvatures.

The phase envelopes of the Eagle Ford oil (with and without capillary pressure) are drawn in **Fig. 10a** and **Fig. 10b** (detail) in the d-T plane and **Fig. 11a** and **Fig. 11b** (a detail, showing also P_w) in the T-P plane. The shift in cricondentherm points is modest for this mixture, only 3 K at r=10 nm and 9 K at r=2 nm. The negative pressures are important, P_z is about -175 bar at low temperatures and P_w is less than -250 bar for r=2 nm.

The phase envelopes in the T-P plane are the practically the same as reported in Sandoval et al. [37] (here the P_w branch is also shown), except for r= 2 nm (in this work there is an inflection point of the bubble point branch at negative pressures and low temperatures). For r=10 nm, the results are very close to those from Ref. [52].

A plot of incipient phase molar density against feed molar density is shown in **Fig. 12**. Note the different shape (as compared to **Fig. 3** for the natural gas) for this oil mixture, with the maximum at high density (the differences in phase densities are important around the maximum).

5.4. Bakken and Wolfcamp shale oils

The Bakken shale oil is described by 8 components (four light alkanes, two intermediate and two heavy pseudo-components). The composition, component properties and non-zero BIPs taken from Nojabaei et al. [32] are given in **Table S5**. The PR EoS is used and calculations are performed at r=10 nm (as in Ref. [32]).

The phase envelopes for the bulk fluid and with capillary pressure are represented in the d-T plane in **Fig. 13** and in the T-P plane in **Fig. 14**. At the reservoir temperature (T=389.3 K, marked with a dashed line in Figs. 13 and 14), the bubble point pressure is suppressed by 5 bar and the capillary

pressure is less than 2 bar; the influence of capillary pressure is not important for this mixture at r=10 nm. The difference in cricondentherm points between bulk and capillary cases is 8 K. The results are similar to those reported by Nojabaei et al. [32]; the differences between bulk and capillary cases are smaller than in Teklu et al. [53] (with confinement and capillary pressure).

Li and Sheng [54] adopted the same fluid characterization for the Wolfcamp shale oil, with the composition given in **Table S5**. In the Wolfcamp reservoir, 93.7 % of pores have a capillary radius r<10 nm [54]. Calculations for this mixture are performed using the PR EoS at r=10 nm and r=5 nm.

The phase envelopes are drawn in **Fig. 15** (in the d-T plane) and in **Fig. 16** (in the P-T plane). At the reservoir temperature (T=397 K, marked with a dashed line in Figs. 15 and 16) the bubble point pressure is suppressed by 9 bar for r=10 nm and by 20 bar for r=5 nm and the capillary pressure is 4 bar for r=10 nm and 11 bar for r=5 nm (these differences are smaller than with confinement [54]). The differences in cricondentherm points in presence and absence of capillary pressure are 7 K for r=10 nm and 12 K for r=5 nm.

In the bulk fluid case, for any EoS, the partial derivatives required in the Jacobian matrix by a volume-based approach are simpler than in the conventional (PT) approach. For two-parameter cubic EoS, these derivatives (given in Ref. [24]) have rather simple forms.

The partial derivatives additionally required when capillary pressure is included have very simple forms in the proposed method, while in PT conventional methods the partial derivatives ($\partial P_C / \partial n_i$, $\partial P_C / \partial P_w$ and $\partial P_C / \partial T$) are more complex, since implicit functions are involved. In volume- (or density-) based methods, the simple forms of the partial derivatives are due to the explicit in volume form of the interfacial tension model. For this reason, the volume-based approach seems particularly suited for phase equilibrium calculations including capillary pressure.

The effects of geometrical confinement [55-58] and of adsorption [59], which are important at small capillary radii, are not addressed here. However, the proposed calculation procedure is applicable using modified component critical properties, to account for the critical shift experienced by a confined fluid [55,56] (as a result, the mixture critical point is changing with capillary radius and phase envelopes are shifted towards lower temperatures and pressures with respect to the bulk fluid). A more complex approach is to extend the EoS by introducing a pair of parameters that characterize the molecule-wall interaction intensity (Travalloni et al. [57,58]); in this case the proposed method is applicable using the appropriate functions and derivatives from the modified EoS.

As in the bulk fluid case [24], a simplified version of the proposed method can be obtained by always calculating a saturation temperature at a specified feed molar density (with a unique saturation temperature for a given feed molar density), starting from a low-pressure dew point. Such a simplified

approach can be seen as a volume-based improved version of the density marching method presented in Ref. [10].

The proposed method is implemented by very easy modifications of an existing code for phase envelope construction (described in Ref. [24]), by only adding the simple capillary pressure terms to residual functions (equation 21) and Jacobian matrix (equation 24).

As a final remark, the main advantage of the proposed density-based method as compared to any conventional (pressure-based) method is that the EoS is not solved for volume and the required partial derivatives are simpler in both bulk and capillary parts of the Jacobian matrix. These features may be very attractive for complex thermodynamic models.

6. Conclusions

A recently developed density-based phase envelope construction method has been adapted to include the capillary pressure effects. As compared to a bulk fluid, under capillary pressure influence the phase envelope is reshaped; bubble point pressures are suppressed and the dew point locus is expanded, with a shift of cricondentherm points towards higher temperatures.

The phase envelope is traced in the molar density-temperature plane, where a unique saturation temperature exists at a specified mixture molar density; the phase envelope in the pressure-temperature plane is obtained by calculating explicitly the pressure (which is always a dependent variable) from the equation of state at given temperature and component molar densities on the saturation curve. The EoS is not solved for volume and the required partial derivatives are simpler than in conventional (pressure-based) methods. The proposed method to include capillary pressure in the phase envelope construction can be applied to any pressure-explicit EoS and to any volume-explicit interfacial tension model.

The additional (as compared to the bulk fluid case) partial derivatives containing capillary terms have extremely simple forms, due to the explicit in volume expression of the interfacial tension. It is shown how the method can be implemented with very easy modifications of an existing code for phase envelope construction of bulk fluids.

The proposed method can handle negative pressures (pressure of the reference liquid phase on the bubble point side at low temperatures), unlike in conventional PT methods.

For the mixtures investigated (ranging from natural gases to heavy oils), the computational results are practically identical to those reported in the literature. The computational procedure is robust, there are no problems in crossing the critical region (where interfacial tensions are very low), at important negative pressures or for large capillary pressures (of the order of hundreds bar in some test examples).

List of symbols

C_{ij}	matrix contaning capillary terms
D	TPD function in terms of molar densities
d	mixture molar density (incipient phase)
d_z	mixture molar density (feed)
d_i	molar density of component *i* (incipient phase)
d_{iz}	molar density of component *i* (feed)
E	scaling exponent
f_i	fugacity of component *i*
$\mathbf{J}$	Jacobian matrix
K_i	equilibrium constants
$\overline{K}_i$	modified equilibrium constants
nc	number of components
n_i	mole numbers of component *i* (incipient phase)
n_T	total number of moles
n_{zi}	mole numbers of component *i* (feed)
P	pressure
P_C	capillary pressure
P_w	pressure in the incipient phase
P_z	pressure in the reference phase
R	universal gas constant
r	capillary radius
S	specification
T	temperature
V	volume
v	molar volume
x_i	mole fraction of component *i* in the incipient phase
z_i	feed composition

Greek letters

γ	±1, depending on the reference phase
δ_{ij}	Kronecker delta
ε	tolerance for convergence
Φ_i	residual
φ_i	fugacity coefficient of component *i*
μ_i	chemical potential of component *i*
Π_i	Parachor of component *i*
ρ	mixture molar density
θ	contact angle
σ	interfacial tension
ξ_i	independent variables
Ψ_i	density function of component *i*

ω acentric factor

Subscripts

i,j component index
C capillary
c critical
w incipient phase
z reference phase

Superscripts

T transposed

References

[1] M.L. Michelsen, Saturation points calculations, Fluid Phase Equilib. 23 (1985) 181-192.

[2] L.X. Nghiem, Y.K. Li, R.A. Heidemann, Application of the tangent plane criterion to saturation pressure and temperature computations, Fluid Phase Equilib. 23 (1985) 39-60.

[3] L.E. Baker, K.D. Luks, Critical point and saturation pressure calculations for multipoint systems, Soc. Petrol. Eng. J. 20 (1980) 15-24.

[4] M.L. Michelsen, Calculation of phase envelopes and critical points for multicomponent mixtures, Fluid Phase Equilib. 4 (1980) 1-10.

[5] L. Asselineau, G. Bogdanic, J. Vidal, A versatile algorithm for calculating vapour—liquid equilibria, Fluid Phase Equilib. 3 (1979) 273-290.

[6] Y.-K. Li, L.X. Nghiem, The development of a general phase envelope construction algorithm for reservoir fluid studies, paper SPE-11198-MS, SPE Annual Technical Conference and Exhibition, 26-29 September, New Orleans, Louisiana, 1982. doi.org/10.2118/11198-MS

[7] R.G. Ziervogel, B.E. Poling, A simple method for constructing phase envelopes for multicomponent mixtures, Fluid Phase Equilib. 11 (1983) 127-135.

[8] D.V. Nichita, Phase envelope construction for mixtures with many components, Energy & Fuels 22 (2008) 488-495.

[9] I.K. Nikolaidis, I.G. Economou, G.C. Boulougouris, L.D. Peristeras, Calculation of the phase envelope of multicomponent mixtures with the bead spring method, AIChE J. 62 (2016) 868–879.

[10] G. Venkatarathnam, Density marching method for calculating phase envelopes, Ind. Eng. Chem. Res. 53 (2014) 3723-3730.

[11] M.L. Michelsen, State function based flash specifications, Fluid Phase Equilib. 158-160 (1999) 617-626.

[12] N.R. Nagarajan, A.S. Cullik, A. Griewank, New strategy for phase equilibrium and critical point calculations by thermodynamic energy analysis. Part I. Stability analysis and flash, Fluid Phase Equilib. 62 (1991) 191-210.

[13] U.K. Deiters, T. Kraska, High-Pressure Fluid Phase Equilibria: Phenomenology and Computation, Vol. 2, 1st Edition, Elsevier, Oxford, 2012. (pp.142-150)

[14] J. Mikyška, A. Firoozabadi, Investigation of mixture stability at given volume, temperature, and number of moles, Fluid Phase Equilib. 321 (2012), 1-9.

[15] D.V. Nichita, Fast and robust phase stability testing at isothermal-isochoric conditions, Fluid Phase Equilib. 447 (2017) 107-124.

[16] D.V. Nichita, A volume-based approach to phase equilibrium calculations at pressure and temperature specifications, Fluid Phase Equilib. 461 (2018) 70-83.

[17] T. Jindrová, J. Mikyška, Fast and robust algorithm for calculation of two-phase equilibria at given volume, temperature, and moles, Fluid Phase Equilib. 353 (2013) 101-114.

[18] M. Castier, Helmholtz function-based global phase stability test and its link to the isothermal-isochoric flash problem, Fluid Phase Equilib. 379 (2014) 104-111.

[19] D.V. Nichita, Volume-based phase stability testing at pressure and temperature specifications, Fluid Phase Equilib. 458 (2018) 123-141.

[20] O. Kunz, R. Klimeck, W. Wagner, M. Jaeschke, The GERG-2004 Wide-Range Equation of State for Natural Gases and Other Mixtures, VDI Verlag GmbH, Düsseldorf, 2007.

[21] S.E. Quinones-Cisneros, U.K. Deiters, An efficient algorithm for the calculation of phase envelopes of fluid mixtures, Fluid Phase Equilib. 329 (2012) 22-31.

[22] U.K. Deiters, Differential equations for the calculation of isopleths of multicomponent fluid mixtures, Fluid Phase Equilib. 447 (2017) 72-83.

[23] I.H. Bell, U.K. Deiters, On the construction of binary mixture p-x and T-x diagrams from isochoric thermodynamics, AIChE J. (2018). DOI: 10.1002/aic.16074

[24] D.V. Nichita, Density-based phase envelope construction, Fluid Phase Equilib. 478 (2018) 100-113.

[25] M.L. Michelsen, The isothermal flash problem. Part I. Stability, Fluid Phase Equilib. 9 (1982) 1-20.

[26] D.V. Nichita, D. Broseta, F. Montel, Calculation of convergence pressure/temperature and stability test limit loci of mixtures with cubic equations of state, Fluid Phase Equilib. 261 (2007) 176-184.

[27] A. Shapiro, E.H. Stenby, Thermodynamics of the multicomponent vapor - liquid equilibrium under capillary pressure difference. Fluid Phase Equilib. 178 (2001) 17-32.

[28] D.R. Sandoval, W. Yan, M.L. Michelsen, The phase envelope of multicomponent mixtures in the presence of a capillary pressure difference, Ind. Eng. Chem. Res. 55 (2016) 6530-6538.

[29] M. Sherafati, K. Jessen, Stability analysis for multicomponent mixtures including capillary pressure, Fluid Phase Equilib. 433 (2017) 56-66.

[30] Y. Li, J. Kou, S. Sun, Thermodynamically Stable Two-Phase Equilibrium Calculation of Hydrocarbon Mixtures with Capillary Pressure, Ind. Eng. Chem. Res. 57 (2018) 17276-17288.

[31] A.I. Brusilovsky, Mathematical simulation of phase behavior of natural multicomponent systems at high pressures with an equation of state, SPE Reservoir Eng. 7 (1992) 117-122.

[32] B. Nojabaei, R.T. Johns, L. Chu, Effect of Capillary Pressure on Phase Behavior in Tight Rocks and Shales, SPE Reservoir Eval. Eng. 16 (2013) 281-289.

[33] J. Pang, J. Zuo, D. Zhang, L. Du, Effect of Porous Media on Saturation Pressures of Shale Gas and Shale Oil, IPTC-16419-MS, International Petroleum Technology Conference, 26-28 March, Beijing, China, 2013. DOI: 10.2523/IPTC-16419-MS

[34] B. Li, A.G. Mezzatesta, H.F. Thern, H. Zhang, J. Wu, B. Zhang, The Condition of Capillary Condensation and Its Effects on Gas-In-Place of Unconventional Gas Condensate Reservoirs, SPE 170837-MS, SPE Annual Technical Conference and Exhibition, 27-29 October, Amsterdam, The Netherlands, 2014. DOI: 10.2118/170837-MS

[35] J.Y. Zuo , X. Guo, Y. Liu, S. Pan, J. Canas, O.C. Mullins, Impact of Capillary Pressure and Nanopore Confinement on Phase Behaviors of Shale Gas and Oil, Energy Fuels 32 (2018) 4705-4714.

[36] C. Lu, Z. Jin, H.A. Li, A two-phase flash algorithm with the consideration of capillary pressure at specified mole numbers, volume and temperature, Fluid Phase Equilib. 485 (2019) 67-82.

[37] D.R. Sandoval, M.L. Michelsen, W. Yan, E.H. Stenby, VT-Based Phase Envelope and Flash Calculations in the Presence of Capillary Pressure, Ind. Eng. Chem. Res. 58 (2019), 5291–5300.

[38] D.V. Nichita, C. Duran-Valencia, S. Gomez, Volume-based thermodynamics global phase stability analysis, Chem. Eng. Commun. 193 (2006) 1194-1216.

[39] D.V. Nichita, J.C. de Hemptinne, S. Gomez, Isochoric phase stability testing for hydrocarbon mixtures, Petrol. Sci. Technol. 27 (2009) 2177–2191.

[40] D.B. Macleod, On a relation between surface tension and density, Trans. Faraday Soc. 19 (1923) 38-41.

[41] S. Sugden, A relation between surface tension, density, and chemical composition, J. Chem. Soc., Trans. 125 (1924) 1177.

[42] C.F. Weinaug, D.L. Katz, Surface tensions of methane-propane mixtures, Ind. Eng. Chem. 35 (1943) 239-246.

[43] D. Broseta, Y. Melean, C. Miqueu, Parachors of liquid/vapor systems: A set of critical amplitudes, Fluid Phase Equilib. 233 (2005) 86-95.

[44] E. Santiso, A. Firoozabadi, Curvature dependency of surface tension in multicomponent systems, AIChE J. 52 (2006) 311-322.

[45] D.V. Nichita, Volume-based phase stability analysis including capillary pressure, Fluid Phase Equilib. 492 (2019) 145-160.

[46] J. Kou, S. Sun, A stable algorithm for calculating phase equilibria with capillarity at specified moles, volume and temperature using a dynamic model, Fluid Phase Equilib. 456 (2018) 7-24.

[47] G. Wilson, A modified Redlich-Kwong equation of state, application to general physical data calculations, the AIChE 65th National Meeting, Cleveland, Ohio, May 4-7, 1969.

[48] G. Soave, Equilibrium constants from a modified Redlich-Kwong equation of state. Chem. Eng. Sci. 27 (1972) 1197-1203.

[49] D.Y. Peng, D.B. Robinson, A new two-constant equation of state. Ind. Eng. Chem. Fund. 15 (1976) 59-64.

[50] D.B. Robinson, D.Y. Peng, 1978, The characterization of the heptanes and heavier fractions for the GPA Peng-Robinson programs, Gas Processors Association, Research Report RR-28.

[51] A. Orangi, N.R. Nagarajan, M.M. Honarpour, J.J. Rosenzweig, Unconventional Shale Oil and Gas-Condensate Reservoir Production, Impact of Rock, Fluid, and Hydraulic Fractures, SPE-140536-MS, SPE Hydraulic Fracturing Technology Conference, 24-26 January, The Woodlands, Texas, USA, 2011. DOI: 10.2118/170837-MS

[52] Y. Xiong, P. Winterfeld, C. Wang, Z. Huang, Y.S. Wu, Effect of Large Capillary Pressure on Fluid Flow and Transport in Stress-sensitive Tight Oil Reservoirs, SPE-175074-MS, SPE Annual Technical Conference and Exhibition, 28-30 September, Houston, Texas, USA, 2015. doi: 10.2118/175074-MS

[53] T.W. Teklu, N. Alharthy, H. Kazemi, X. Yin, R.M. Graves, A.M. AlSumaiti, Phase Behavior and Minimum Miscibility Pressure in Nanopores, SPE Reservoir Eval. Eng. 17 (2014) 396-403.

[54] L. Li, J.J. Sheng, Nanopore confinement effects on phase behavior and capillary pressure in a Wolfcamp shale reservoir, J. Taiwan Inst. Chem. Eng. 78 (2017) 317-328.

[55] G.J. Zarragoicoechea, V.A. Kuz, Critical shift of a confined fluid in a nanopore, Fluid Phase Equilib. 220 (2004) 7-9.

[56] S.K. Singh, A.Sinha, G. Deo, J.K. Singh, Vapor-Liquid Phase Coexistence, Critical Properties, and Surface Tension of Confined Alkanes, J. Phys. Chem. C 113 (2009) 7170-7180.

[57] L. Travalloni, M. Castier, F. W. Tavares, S.I. Sandler, Thermodynamic modeling of confined fluids using an extension of the generalized van der Waals theory, Chem. Eng. Sci. 65 (2010) 3088-3099.

[58] L. Travalloni, M. Castier, F.W. Tavares, Phase equilibrium of fluids confined in porous media from an extended Peng–Robinson equation of state, Fluid Phase Equilib. 362 (2014) 335-341.

[59] D.R. Sandoval, W. Yan, M.L. Michelsen, E.H. Stenby, Influence of Adsorption and Capillary Pressure on Phase Equilibria inside Shale Reservoirs, Energy Fuels, 32 (2018) 2819-2833.

Table 1 Mixture critical points

Mixture	T_c, K	P_c, bar	d_c, Kmol/m^3
M7	203.238	58.934	11.1386
SJ15 oil	721.343	114.674	2.2478
SJ15 gas cond.	239.655	105.353	13.4235
Eagle Ford	712.762	101.819	2.1161
Bakken	584.451	259.255	5.4770
Wolfcamp	661.082	226.676	4.2890

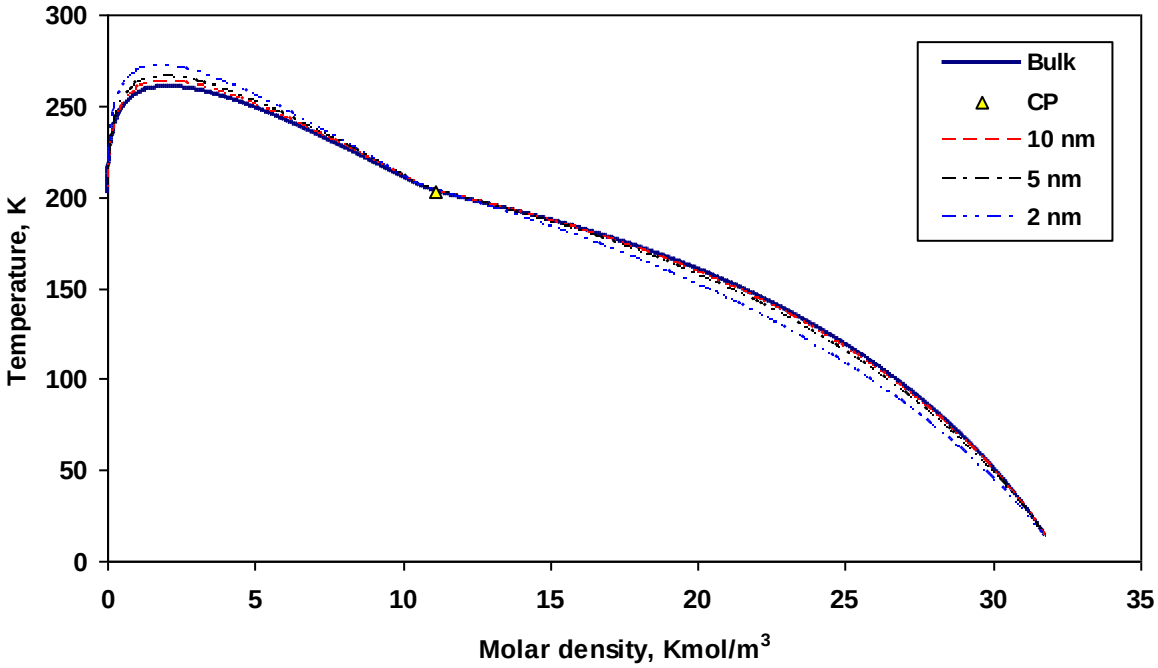

(a)

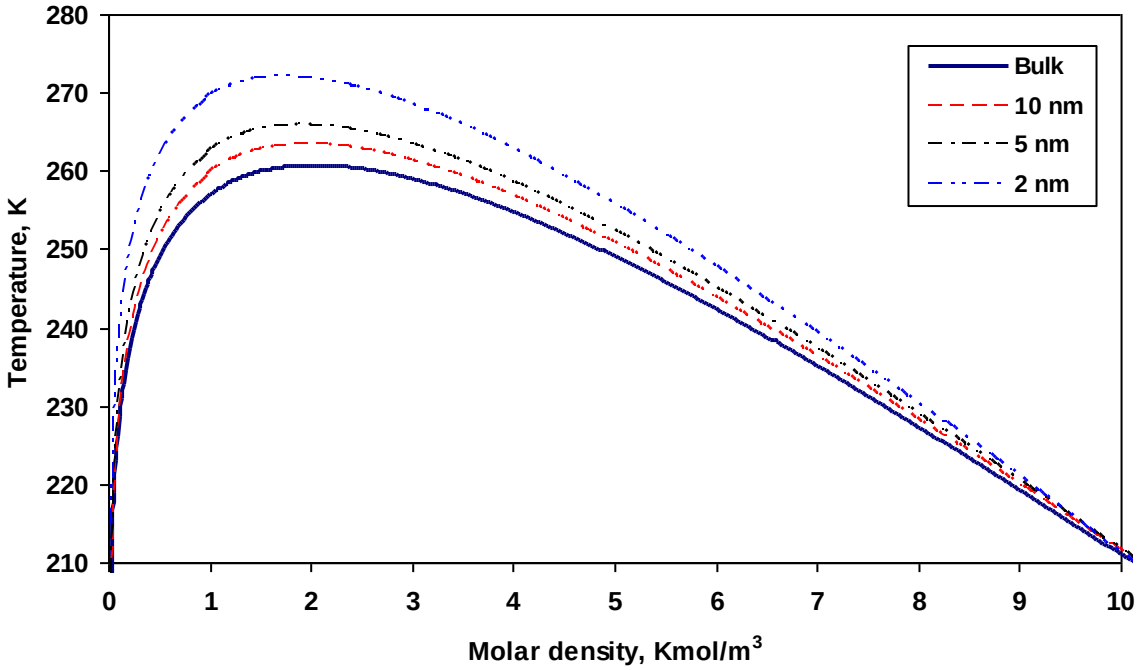

(b)

Fig. 1 Phase envelope of M7 natural gas. (a) d-T plane; (b) d-T plane (detail)

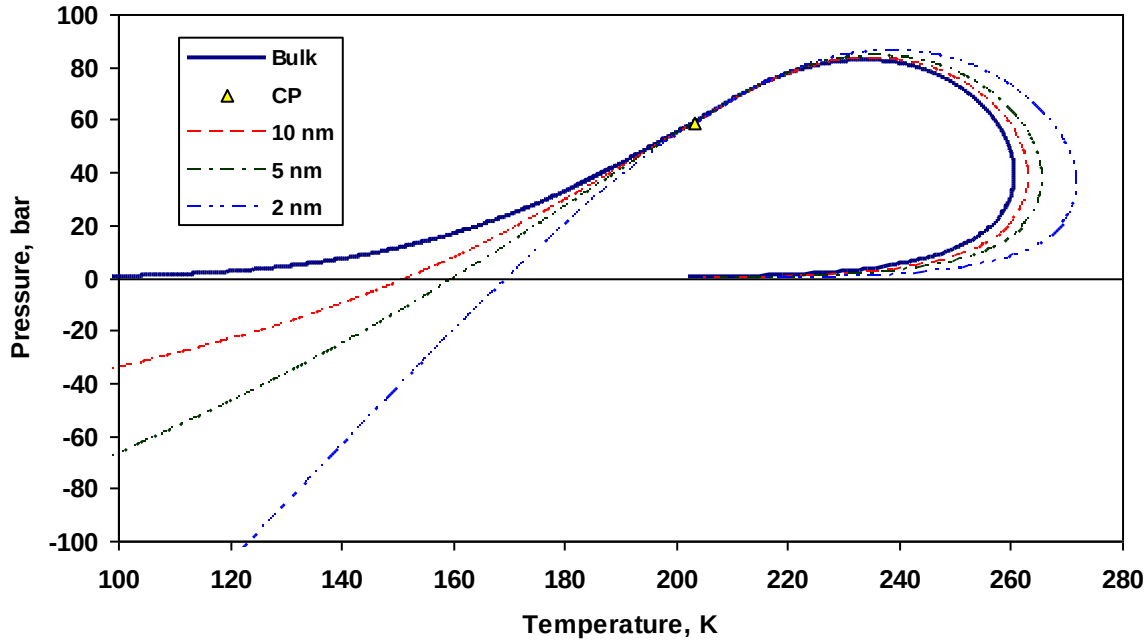

(a)

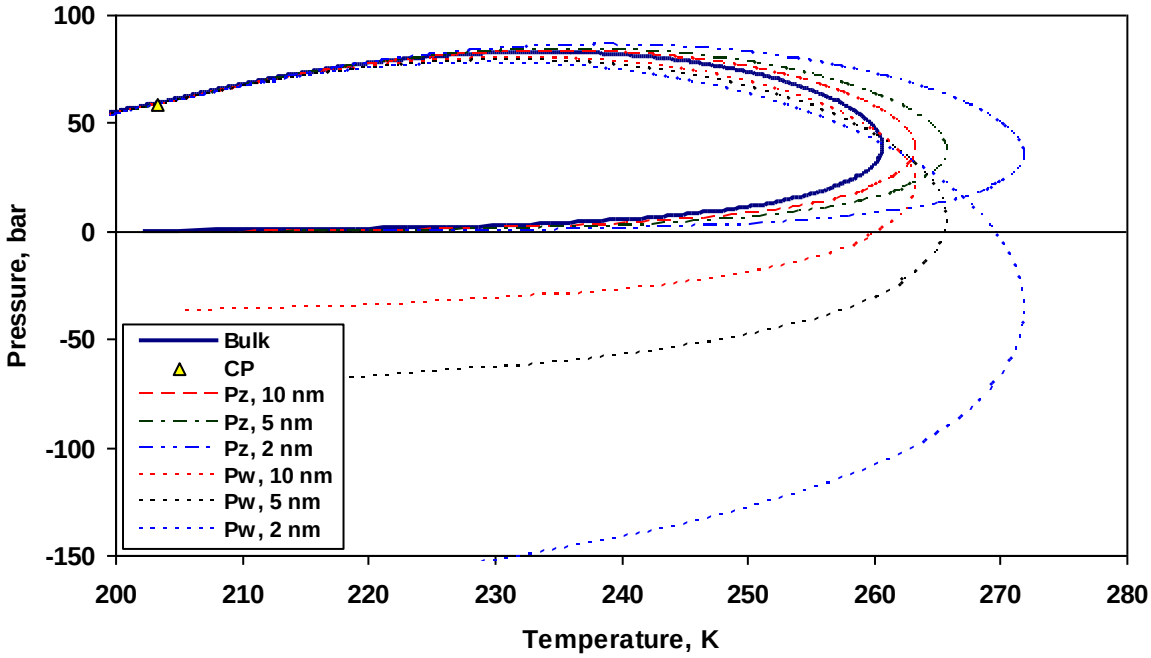

(b)

Fig. 2 Phase envelope of M7 natural gas. (a) T-P plane; (b) T-P plane (detail)

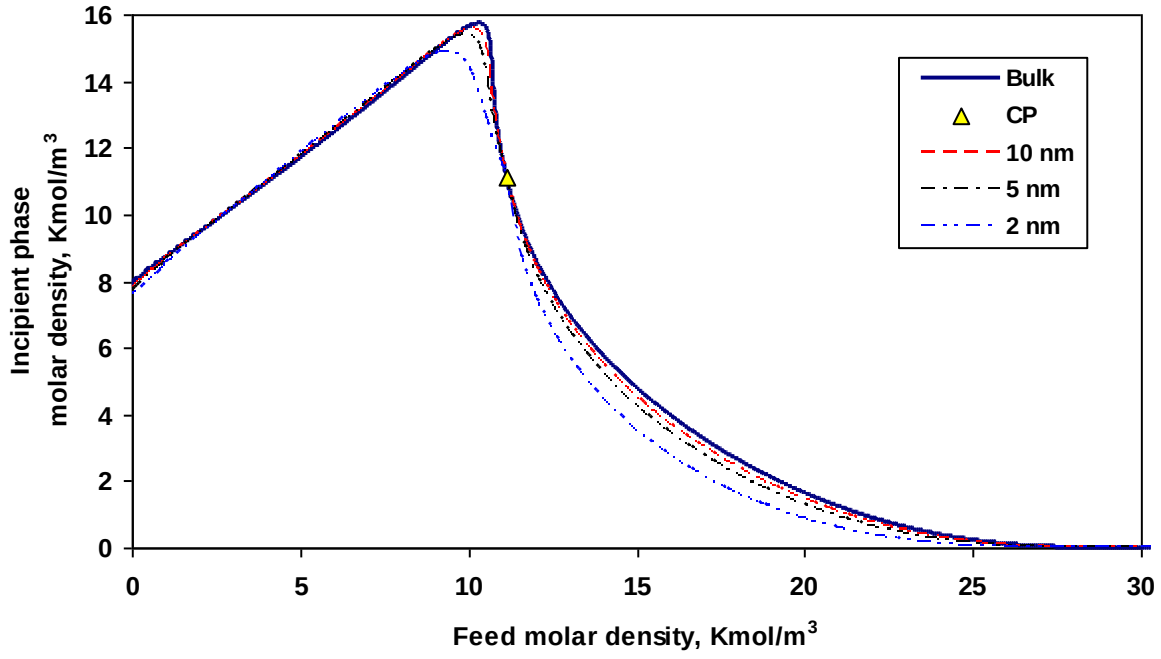

Fig. 3 Incipient phase vs. feed molar densities for the M7 natural gas

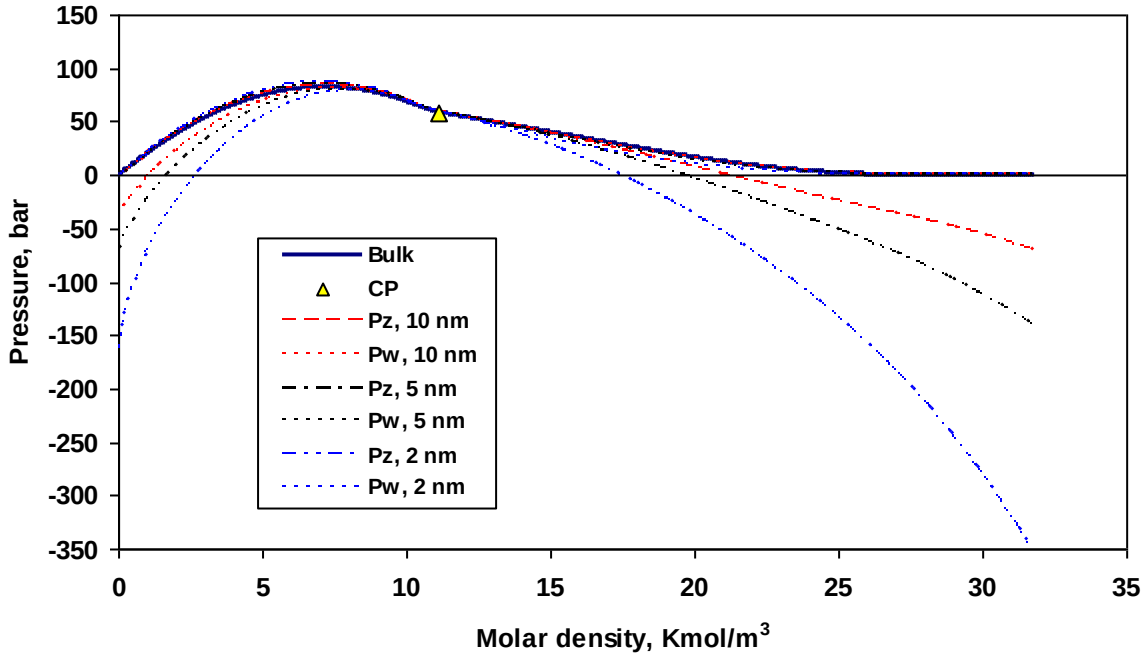

Fig. 4 Phase envelope of M7 natural gas in the d-P plane

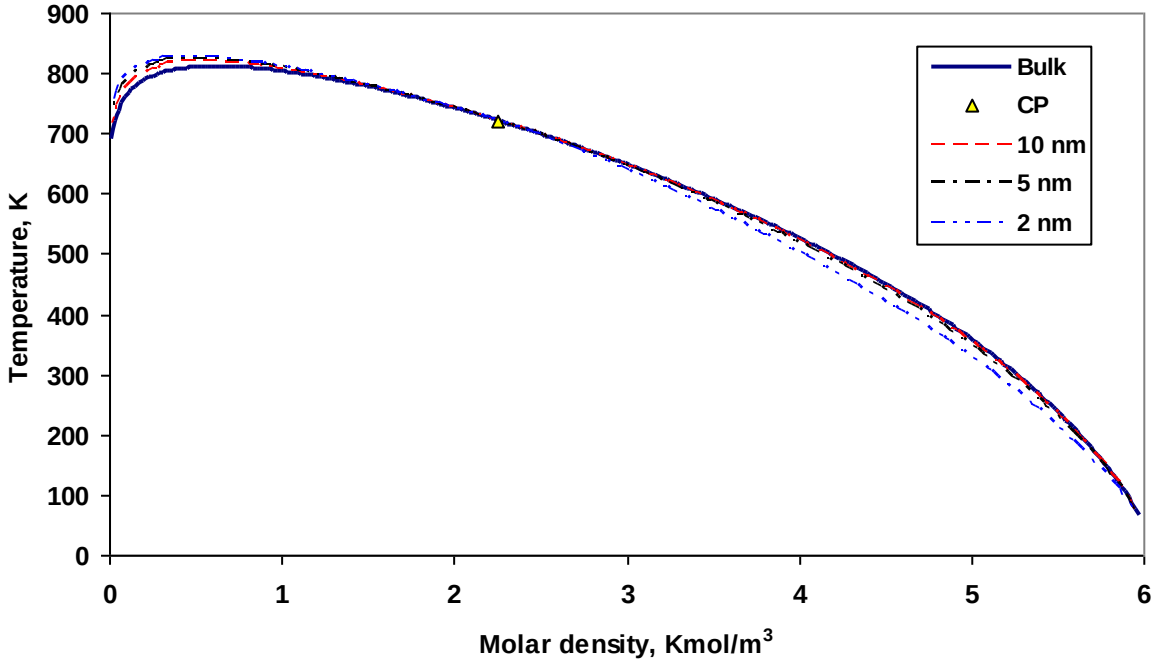

(a)

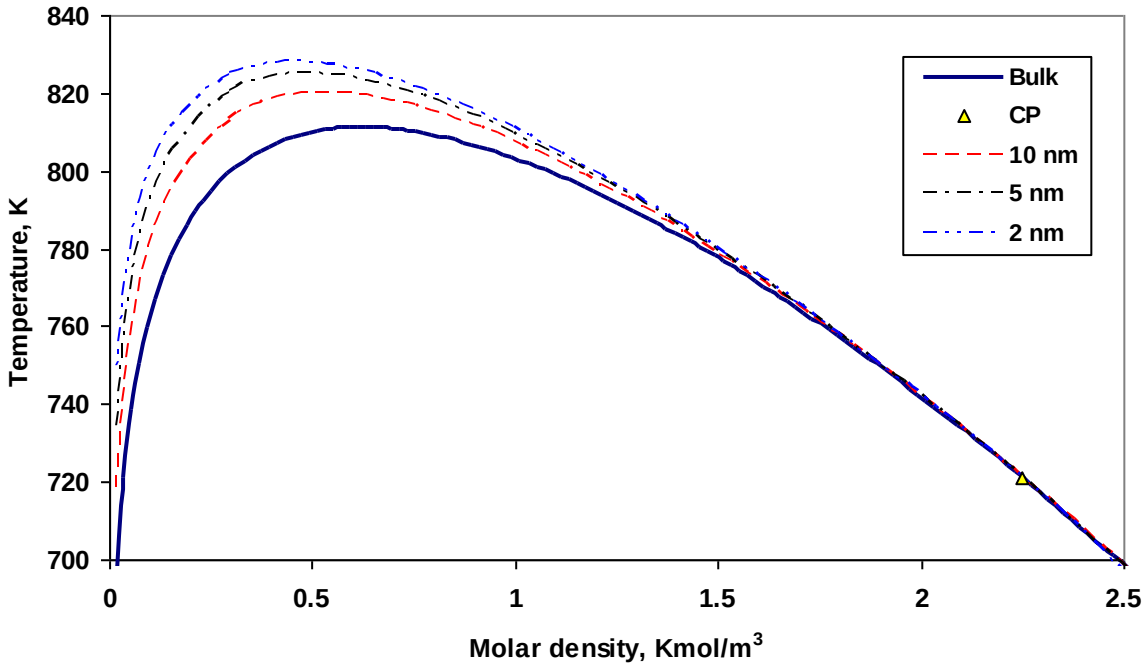

(b)

Fig. 5 Phase envelope of SJ15 oil. (a) d-T plane; (b) d-T plane (detail)

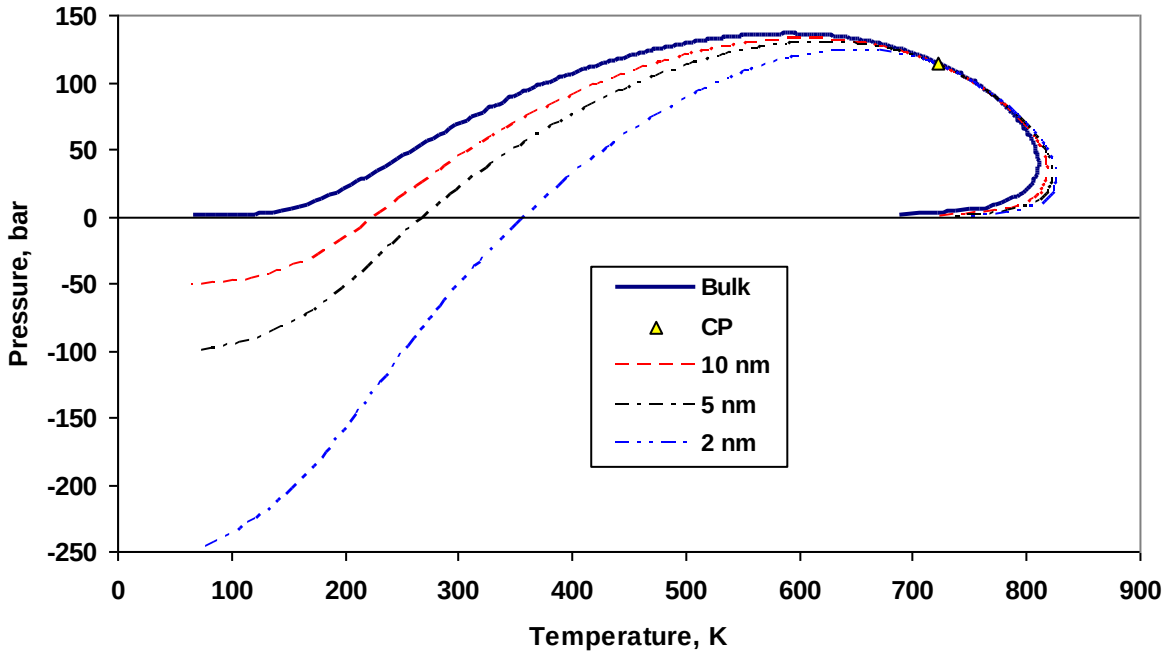

Fig. 6 Phase envelope of SJ15 oil in the T-P plane

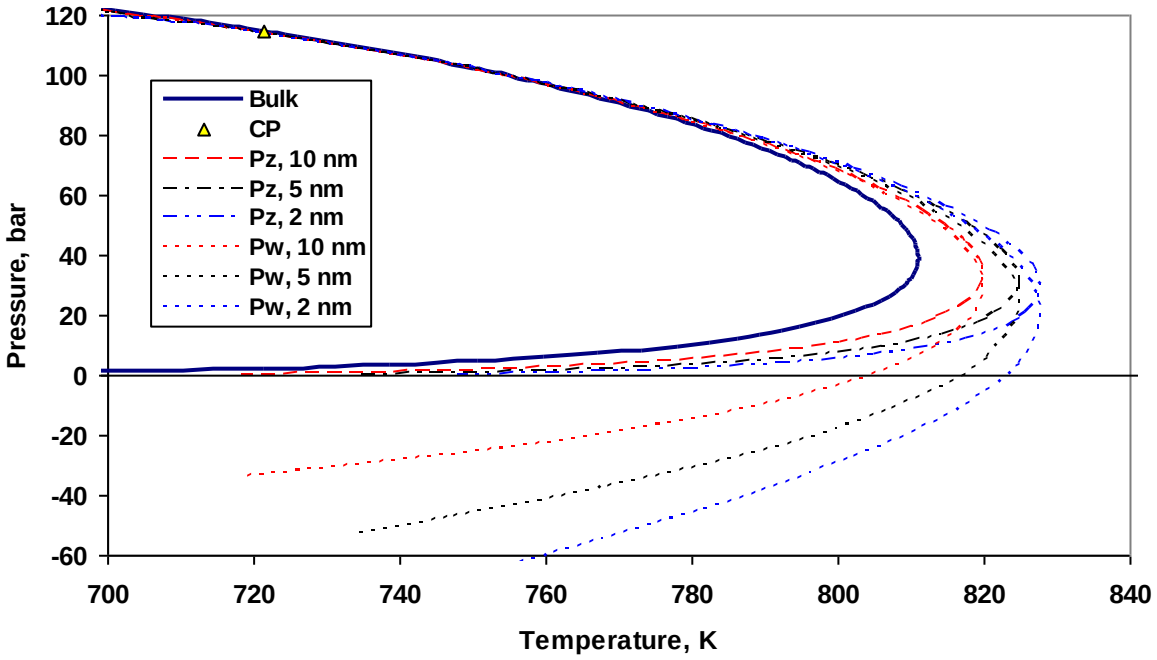

(a)

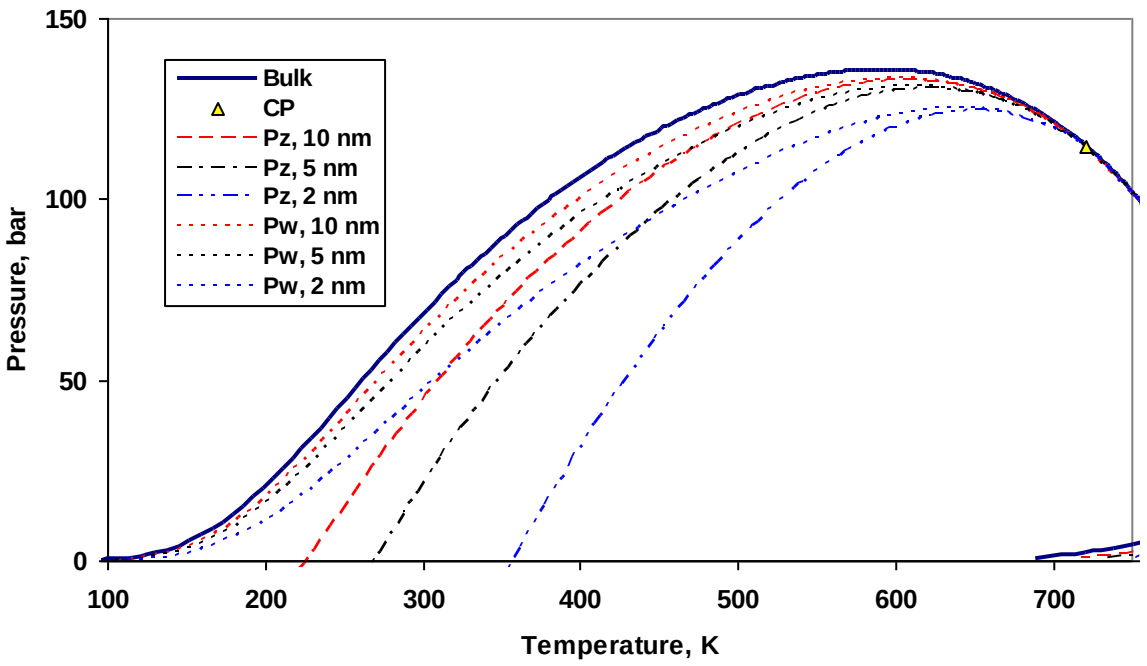

(b)

Fig. 7 Phase envelope of SJ15 oil. (a) T-P plane (detail on the dew point side); (b) T-P plane (detail on the bubble point side)

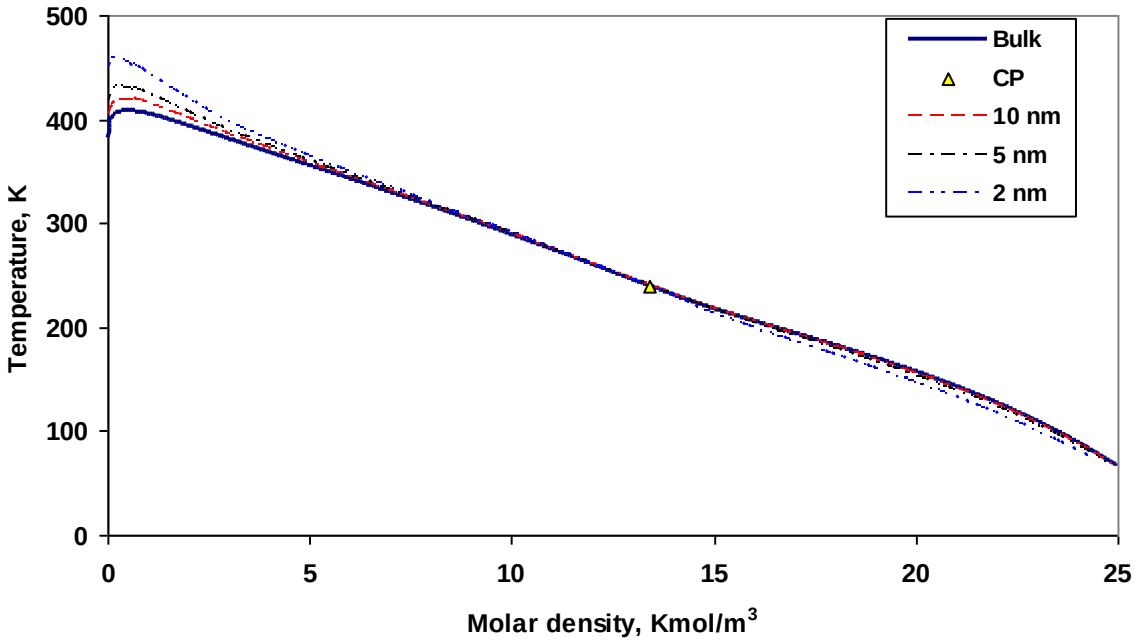

(a)

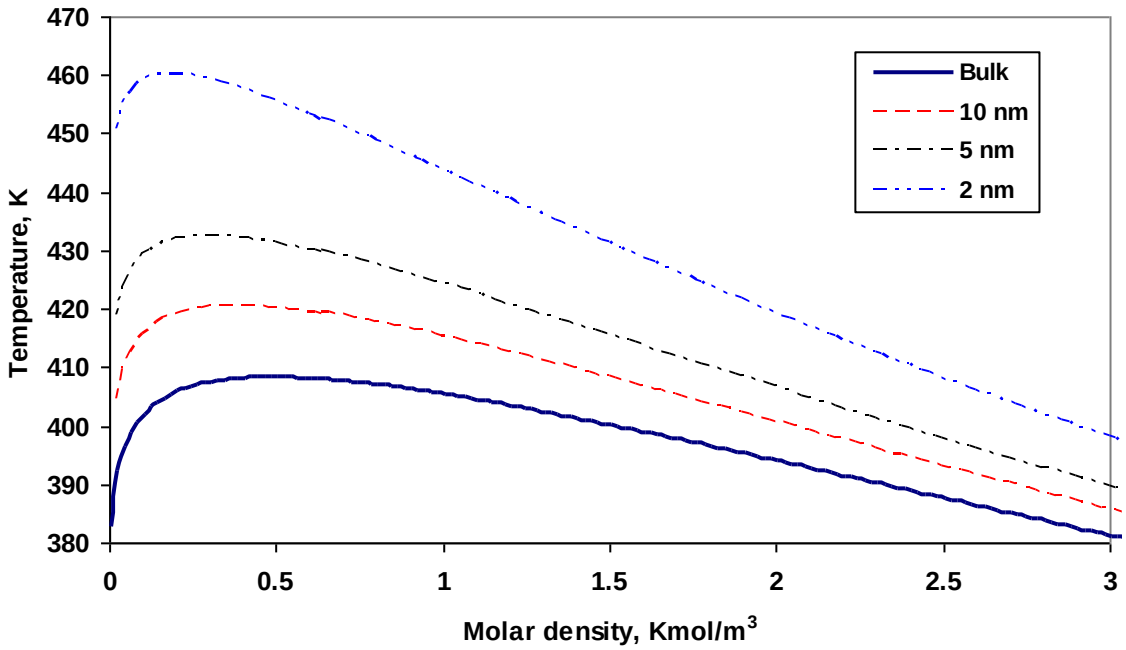

(b)

Fig. 8 Phase envelope of SJ15 gas-condensate. (a) d-T plane; (b) d-T plane (detail)

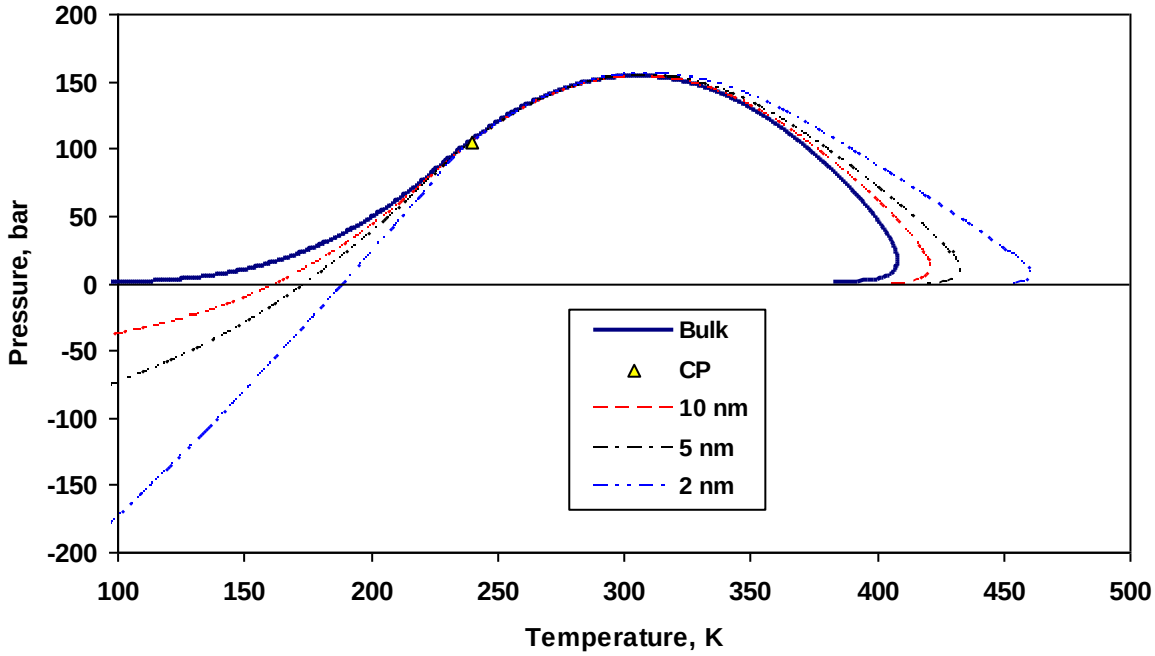

(a)

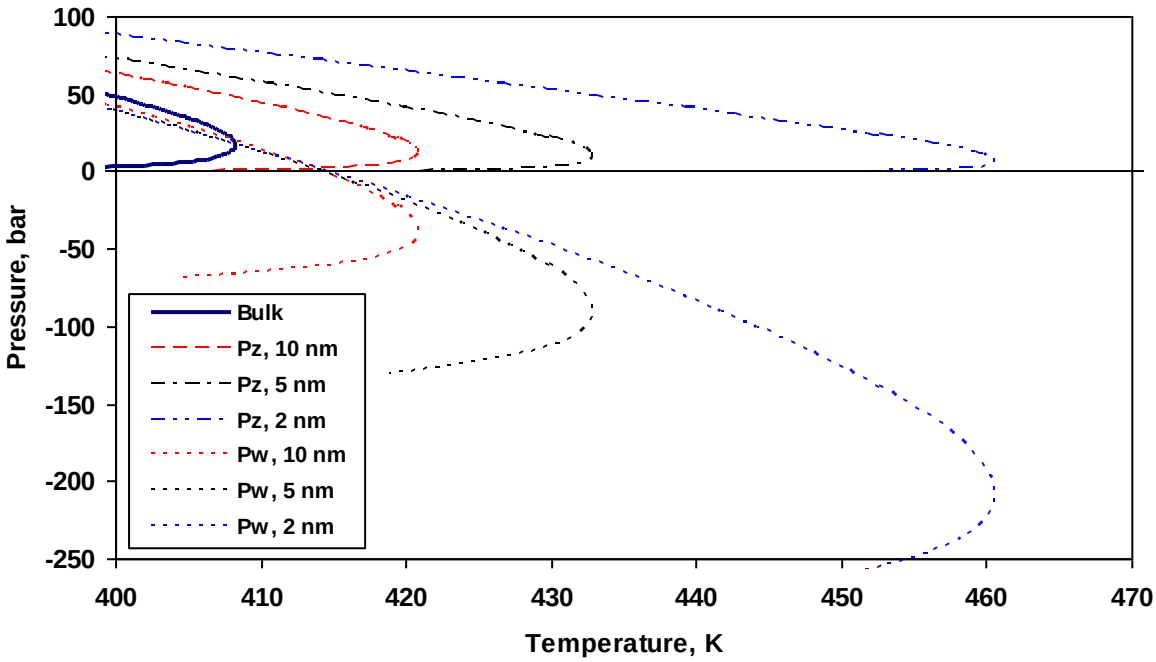

(b)

Fig. 9 Phase envelope of SJ15 gas-condensate. (a) T-P plane; (b) T-P plane (detail)

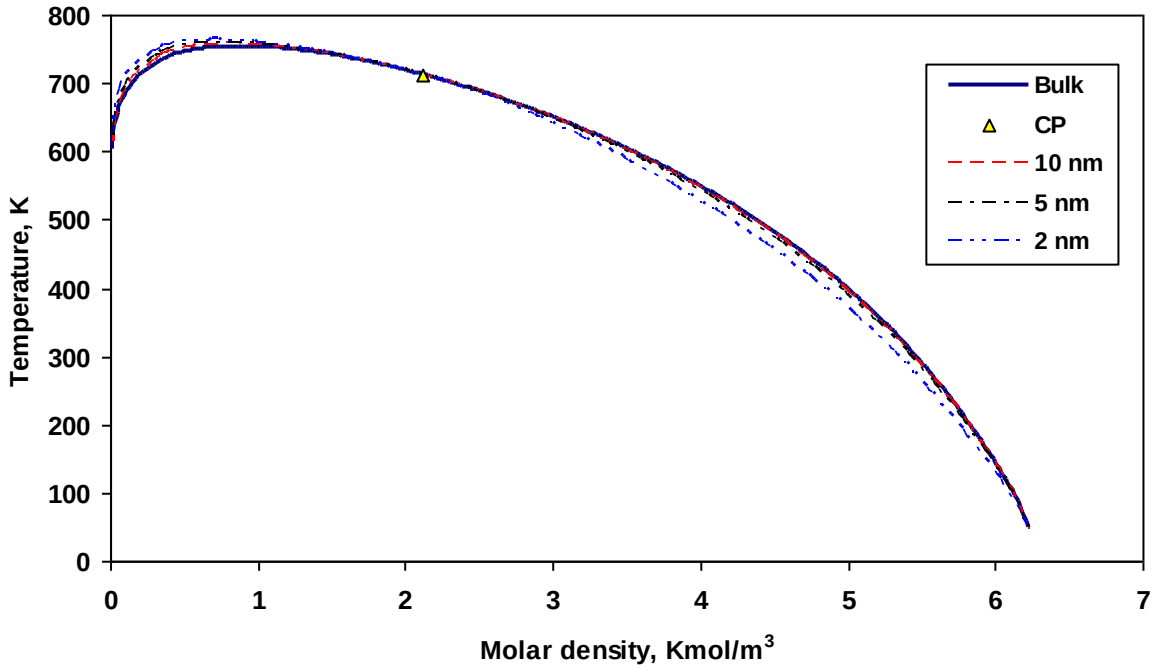

(a)

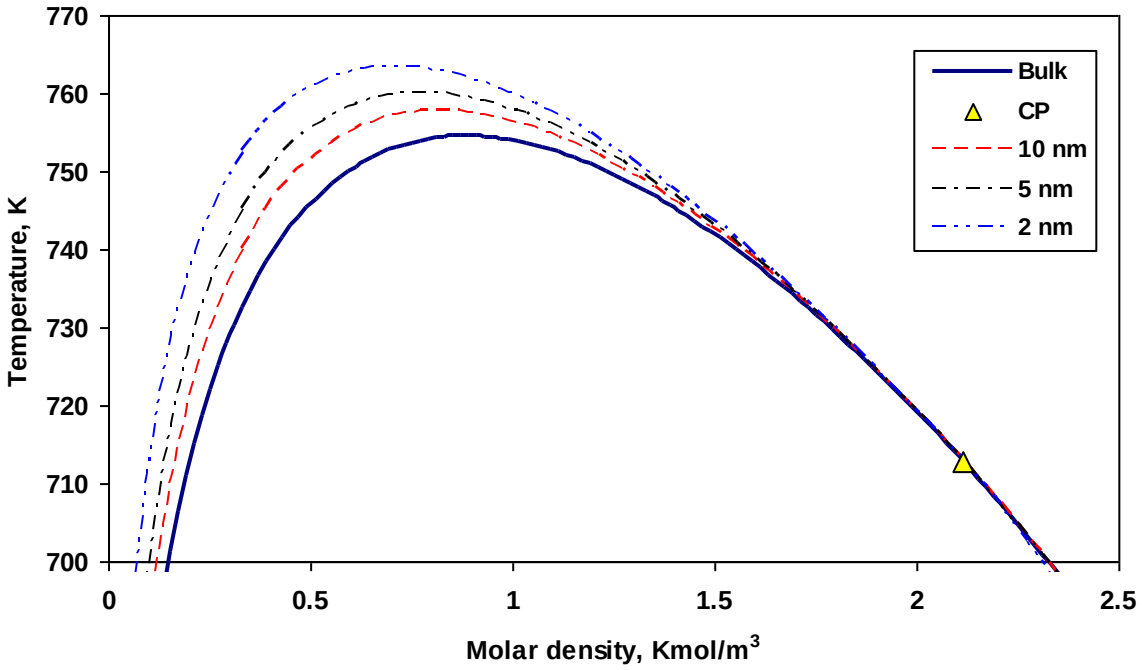

(b)

Fig. 10 Phase envelope of Eagle Ford oil. (a) d-T plane; (b) d-T plane (detail)

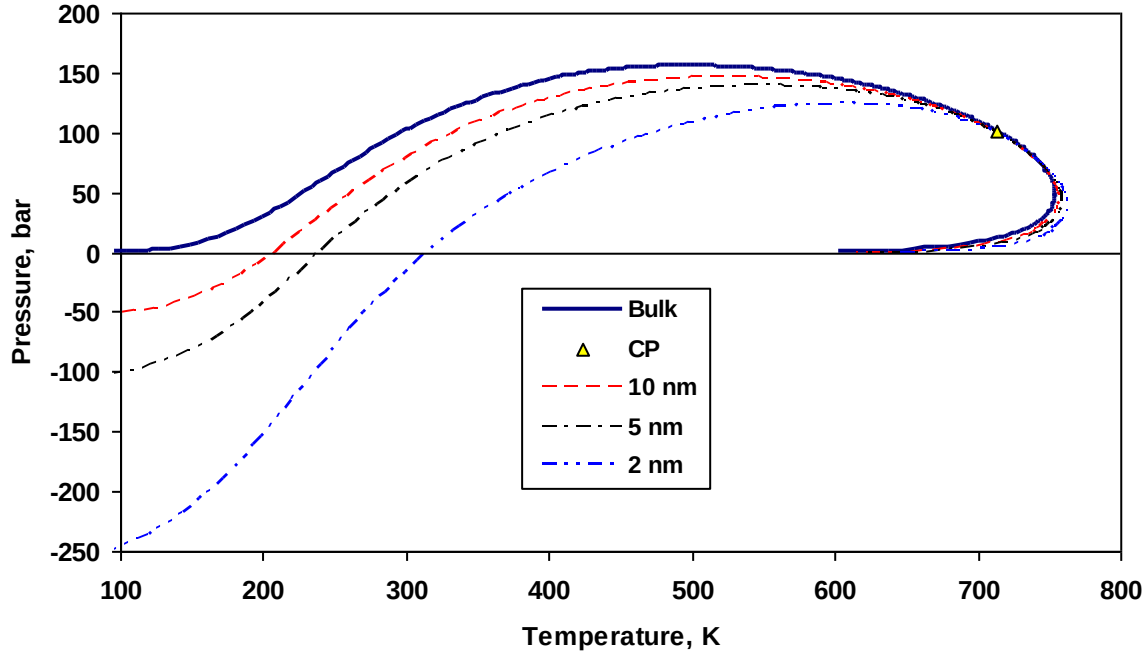

(a)

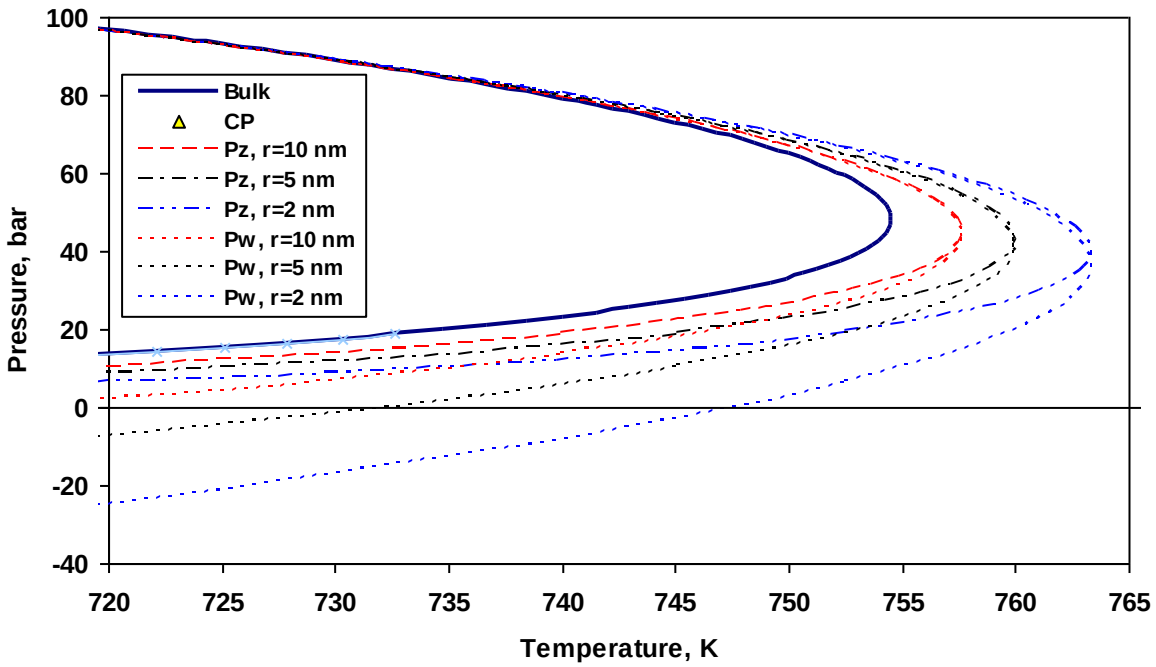

(b)

Fig. 11 Phase envelope of Eagle Ford oil. (a) T-P plane; (b) T-P plane (detail)

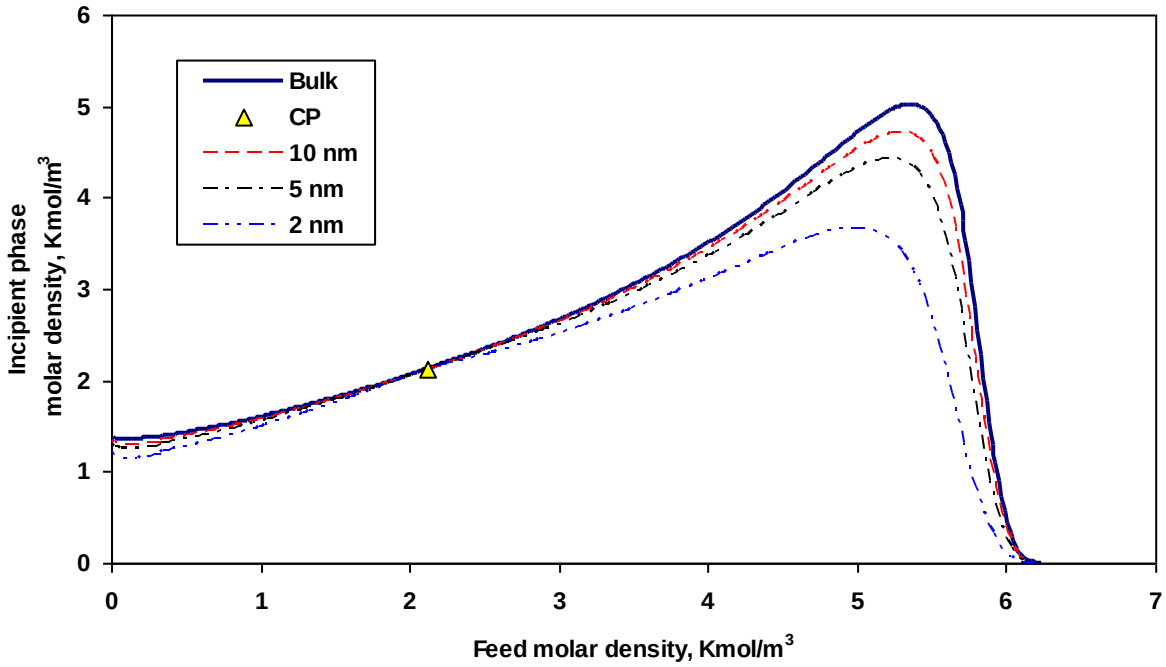

Fig. 12 Incipient phase vs. feed molar densities for the Eagle Ford oil

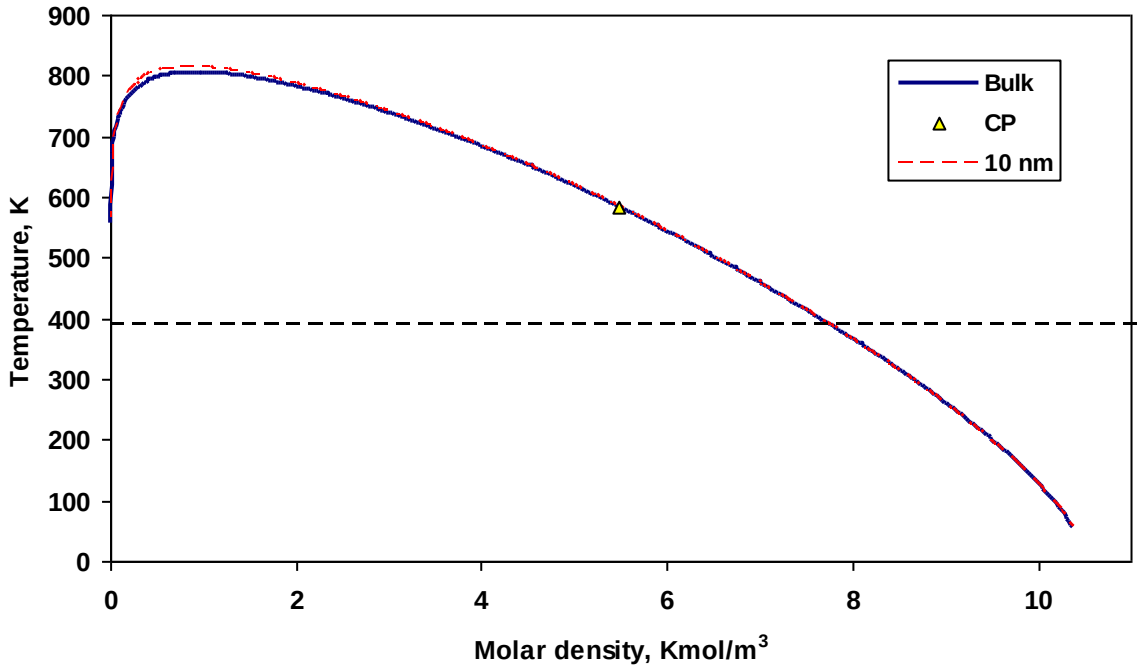

Fig. 13 Phase envelope of Bakken oil in the d-T plane

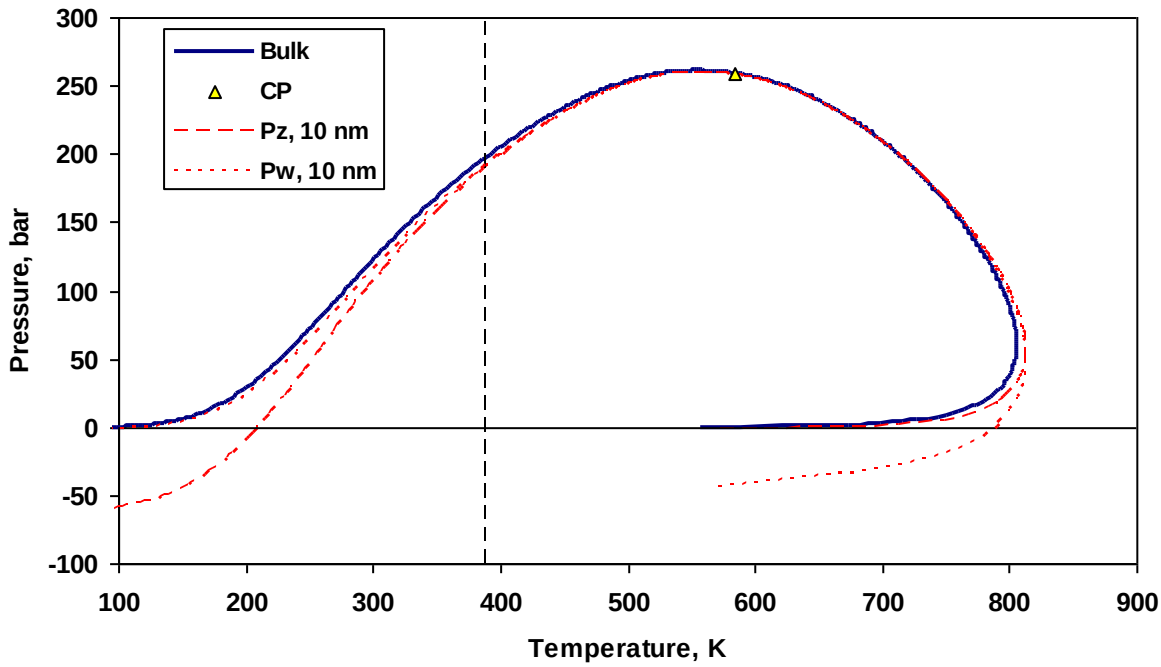

Fig. 14 Phase envelope of Bakken oil in the T-P plane

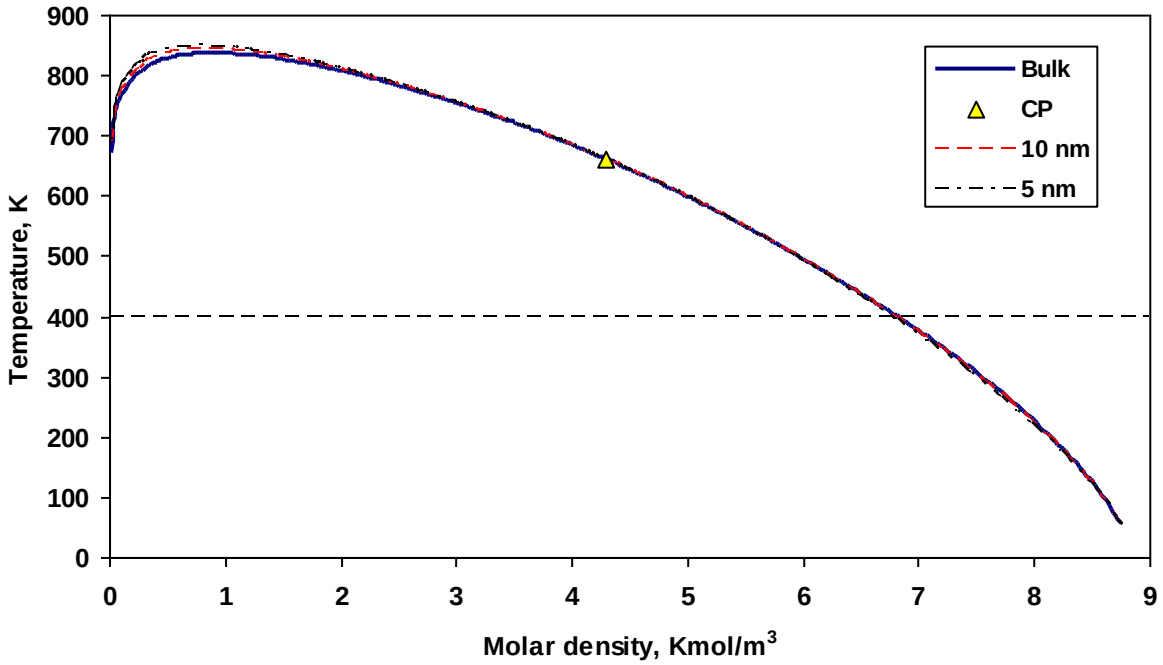

Fig. 15 Phase envelope of Wolfcamp oil in the d-T plane

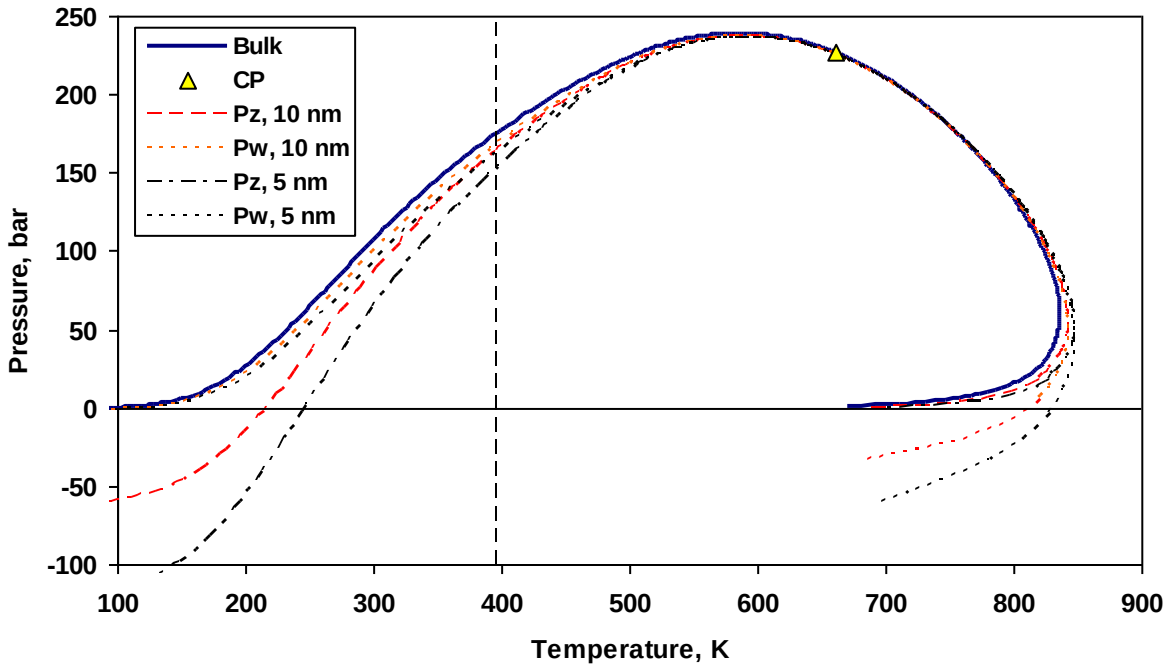

Fig. 16 Phase envelope of Wolfcamp oil in the T-P plane